Moore, G.F., Taira, A., and Klaus, A. (Eds.)
Proceedings of the Ocean Drilling Program, Initial Reports Volume 190

3. Explanatory Notes[1]

Shipboard Scientific Party[2]

INTRODUCTION

This chapter includes information on shipboard methods that will help the reader understand the basis for our preliminary interpretations and also help the interested investigator select samples for further analysis. Coring techniques and core handling, including the numbering of sites, holes, cores, sections, and samples (Fig. F1), are the same as those reported in previous *Initial Reports* volumes of the *Proceedings of the Ocean Drilling Program* and are only briefly summarized.

Authorship of Site Chapters

The separate sections of the site chapters were written by the following shipboard scientists (authors are listed in alphabetical order; no seniority is implied):

Principal Results: Shipboard Scientific Party
Operations: Pettigrew, Klaus
Lithostratigraphy: Fergusson, Hirano, Stuerer, Wilson, Underwood
Structural Geology: Maltman, Morgan, Sanchez-Gomez, Tobin, Ujiie
Biostratigraphy: Boeckel
Paleomagnetism: Dean, Hisamitsu
Inorganic Geochemistry: Kastner, Spivack
Organic Geochemistry: L. Becker
Microbiology: Cragg, Murakami, Smith
Physical Properties: Henry, Hunze, Saffer, Screaton
Downhole Measurements: Tobin
In Situ Temperature Measurements: K. Becker, Screaton
Seismic Stratigraphy: Moore

F1. Diagram illustrating core, section, and sample numbering, p. 33.

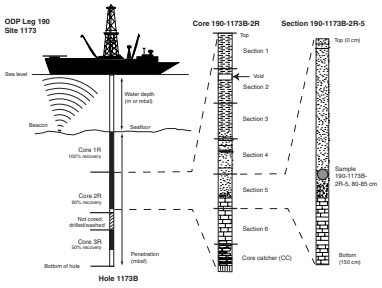

[1]Examples of how to reference the whole or part of this volume.
[2]Shipboard Scientific Party addresses.

Ms 190IR-103

Reference Depths

Seafloor depths and cored intervals below seafloor (meters below seafloor [mbsf]) are determined by drill-pipe measurement.

Numbering of Sites, Holes, Cores, Sections, and Samples

Drill sites are numbered consecutively from the first site drilled by the *Glomar Challenger* in 1968. A site refers to one or more holes drilled while the ship was positioned over a single acoustic beacon. The first hole drilled at a given site is assigned the site number modified by the suffix "A," the second hole takes the site number and suffix "B," and so forth. These suffixes are assigned regardless of recovery, as long as penetration takes place.

Each cored interval is generally 9.5 m long, which is the length of a core barrel. Coring intervals may be shorter and may not necessarily be adjacent if separated by intervals drilled but not cored. The depth interval assigned to an individual core begins with the depth below the seafloor at which the coring operation began and extends to the depth that the coring operation ended for that core.

A recovered core is typically divided into 1.5-m-long sections that are numbered serially from 1 through 7 (or less if partial recovery) beginning at the top. When the recovered core is shorter than the cored interval, the top of the core is equated with the top of the cored interval by convention in order to achieve consistency in handling analytical data derived from the cores. Also by convention, material recovered from the core catcher is placed in a separate section during the core description, labeled core catcher (CC), and placed below the last (bottom) section recovered in the liner. The core catcher is placed at the top of the cored interval in cases where material is only recovered in the core catcher.

Samples removed from a core section are designated by distance measured in centimeters from the top of the section to the top and bottom of each sample removed from that section. A full identification number for a sample consists of the following information: leg, site, hole, core number, core type, section number, and top to bottom interval in centimeters measured from the top of section. For example, a sample identification of "190-1173B-26R-2, 20–25 cm" represents a sample removed from the interval between 20 and 25 cm below the top of Section 2. Core 26R designates that this core was taken during rotary core barrel coring of Hole 1173B from Leg 190.

All ODP core identifiers indicate core type. The following abbreviations are used: H = advanced hydraulic piston corer (APC); X = extended core barrel (XCB); R = rotary core barrel (RCB).

Core Handling

As soon as a core is retrieved on deck, a sample is taken from the core catcher and, if sedimentary, given to the paleontological laboratory for an initial age assessment. The core liner with the core inside is marked into section lengths, each section is labeled, and the core is cut into sections. If a whole-round sample is to be taken, the desired interval is identified, cut out of the core, and then the section are cut. When possible, these samples are taken from the bottom of sections. During Leg 190, whole-round samples were taken for interstitial water (IW) analy-

ses, organic geochemistry, and microbiology as well as for postcruise permeability and consolidation/strength measurements. For safety monitoring, small (~5 cm^3) plugs of sediment are taken from the end of one section per core for headspace gas analysis. If pockets of gas are present, a vacutainer gas sample is taken through the core liner.

Each section is then sealed at the top and bottom by using acetone to seal color-coded plastic caps to the plastic core liner. A blue end cap marks the top of a section, a clear cap marks the bottom, and a yellow cap marks the end of a section from which a whole-round sample has been removed. The sample code (e.g., IW) is written on the yellow cap. The core sections are then carried into the laboratory, and the length of the core sections and any samples taken are logged into the shipboard database.

After the core sections equilibrate to ambient lab temperature (~3 hr), they are run through the multisensor track (MST). For soft sediments, thermal conductivity measurements are then made (see **"Physical Properties,"** p. 19). Cores are subsequently split lengthwise into working and archive halves. The archive half is used for nondestructive measurements: visual core description, paleomagnetism, magnetic susceptibility, and color reflectance. Samples were taken from the working half for shipboard physical properties measurements (see **"Physical Properties,"** p. 19) before being sampled for additional shipboard and postcruise studies. The archive halves were photographed a whole core at a time, and close-up photographs were taken as requested. Finally, the core sections were put into labeled plastic tubes, sealed, and transferred to cold-storage space aboard the drilling vessel. Following the cruise, the cores were transported to the Gulf Coast Repository of the Ocean Drilling Program (ODP) in College Station, Texas.

LITHOSTRATIGRAPHY

Visual Core Descriptions

We followed normal ODP procedures for recording sedimentologic information on visual core description (VCD) forms on a section-by-section basis (Mazzullo and Graham, 1988). VCD data were transferred to core-scale "barrel sheets" using AppleCORE software (Shipboard Scientific Party, 1997). Textural subdivisions for siliciclastic sediments and the classification scheme for siliciclastic lithologies follow Mazzullo et al. (1988). The "Graphic Lithology" column on each barrel sheet shows to scale all intervals that are at least 10 cm thick. Combined graphic patterns are used to indicate interbeds less than 10 cm thick. Differences between the silty clay and clayey silt lithologies can be subtle and not easily separated without further analysis, so we grouped this entire range of sediment textures into the category "clayey silt" on all barrel sheets. Figure **F2** displays the graphic patterns for all lithologies encountered during Leg 190. Separate patterns have not been used for more heavily indurated examples of the same lithologies (e.g., sand vs. sandstone). Also shown are symbols for internal sedimentary structures, deformation structures, and symbols for core disturbance in both soft sediment and indurated sedimentary rock. The "Samples" column on the barrel sheets indicates the positions and types of samples taken from each core for shipboard analyses. The abbreviations for these samples are as follows: IW = interstitial water; SS = smear slide; WRP = whole round for physical properties; WRB = whole round for microbiol-

F2. Graphic patterns and symbols used on AppleCORE barrel sheets during Leg 190, p. 34.

ogy; WHC = whole-core sample. Using the working half of each core, sediment color was measured at 10-cm intervals with a Minolta CM-2002 Spectrophotometer mounted on an automated scanning table. The specifics of this spectrophotometer were described by Schneider et al. (1995).

Smear Slides

The results of semiquantitative smear-slide analyses are tabulated with visual percentage estimates for each constituent grouped into the following categories: D = dominant (>50%); A = abundant (>20%–50%); C = common (>5%–20%); P = present (>1%–5%); R = rare (0.1%–1%); T = trace (<0.1%). In the "Lithology" column of the data tables, "D" indicates that the sample is representative of the dominant lithology of the core and "M" indicates a minor component. Data were entered into the Sliders computer program.

Thin Sections

Thin sections of sand, volcanic ash, tuff, and basalt were prepared for petrographic analysis, with visual percentage estimates for each constituent grouped into the following categories: D = dominant (>50%); A = abundant (>20%–50%); C = common (>5%–20%); P = present (>1%–5%); R = rare (0.1%–1%); T = trace (<0.1%). Unconsolidated sands were washed of fine-grained matrix using a 63-µm sieve, dried, and impregnated in epoxy. Data were entered into the STP computer program.

X-Ray Diffraction

Routine samples for shipboard X-ray diffraction (XRD) analysis were taken from intervals adjacent to whole-round samples, and most are part of sampling clusters adjacent to physical properties and carbonate samples. Additional samples were collected periodically from such unusual lithologies as carbonate-cemented claystone and volcanic ash. Samples were freeze-dried, crushed either by hand or with a ball mill, and mounted as random bulk powders. The XRD laboratory aboard the *JOIDES Resolution* is equipped with a Philips PW-1729 X-ray generator and a Philips PW-1710/00 diffraction control unit with a PW-1775 35 port automatic sample changer. Machine settings for all standards were as follows: generator = 40 kV and 35 mA; tube anode = Cu; wavelength = 1.54184 Å (CuK_α); intensity ratio = 0.5; focus = fine; irradiated length = 12 mm; divergence slit = fixed at 1°; receiving slit = 0.2 mm; step size = 0.02°2θ; count time per step = 1 s; scanning rate = 2°2θ/min; rate meter constant = 0.2 s; spinner = off; monochronometer = on; scan = step; scanning range = 2°2θ to 40°2θ.

The software used for XRD data reduction is MacDiff (versions 4.0.4 and 4.1.1). This shareware application for Macintosh computers supports digital data processing and measurement of peak geometry. Peak intensity (counts per step) and peak area (total counts) were recorded after creating a baseline (200 iterations for all 2-θ values) and smoothing the counts (17-term filter of standard weighted means).

The method of Fisher and Underwood (1995) was employed to determine semiquantitative relative abundances of minerals. This mathematical technique uses matrix singular value decomposition (SVD) to solve for reliable normalization factors. Calibration depends upon the analysis of known weight percent mixtures of mineral standards that

are appropriate matches for the natural sediments encountered in the Nankai Trough. We emphasize that the normalization factors are specific to the combination of XRD hardware and software utilized during Leg 190. Seven reference minerals were chosen for the standard mixtures: smectite (Wyoming montmorillonite), illite (2M1 polytype), chlorite, kaolinite, quartz (St. Peter sandstone), plagioclase feldspar (Ca-rich albite), and calcite (Cyprus chalk).

Figure F3 shows the positions of all peaks used in semiquantitative analysis of mineral abundance. The numerical technique of Fisher and Underwood (1995) allows one to assign either positive or negative normalization factors to relate each indicator mineral to each target phase (Table T1). Sixteen mixtures of mineral standards were tested; each mixture was split and analyzed three times, and the average peak-area value for each mineral was input into the SVD calculations for each mixture. All XRD-determined abundances were normalized to 100%. Differences between the measured weight percentage for each mineral in the standard mixture and its respective average of XRD-determined weight percentage are generally <5% (Table T2). Average errors range from ±0.8% to ±3.2%. Errors are larger for chlorite + kaolinite and quartz.

As an independent check on the accuracy of SVD-based calculations, we also completed linear regression analysis on the relation between weight percent and peak area for each mineral in the standard mixtures. The smallest correlation coefficients are for smectite (r = 0.90), chlorite + kaolinite (r = 0.92), and quartz (r = 0.95). Errors increase using this technique as the absolute abundance of a particular mineral increases (Table T2). Nevertheless, when applied to data from natural bulk-powder specimens, regression equations for each mineral (Table T3) yielded results that are very similar to those based on SVD. Small systematic shifts occur in quartz (~2% higher using SVD) and plagioclase (~2% lower using SVD). Finally, we also tested the reproducibility of data reduction technique by having multiple operators determine peak areas using MacDiff software. These deviations, on average, are less than 1% and are caused by variations in where peaks intersect with baseline counts.

Limitations of X-ray diffraction analysis, as applied to specifically to sediments from the Nankai Trough, include (1) peak interference between (001) smectite and (001) chlorite; (2) peak interference between (002) chlorite and (001) kaolinite; (3) contamination of the Wyoming montmorillonite standard by quartz, which Fisher and Underwood (1995) estimated to be 39%; heterogeneity of the montmorillonite standard means that this value may not be accurate for all subsamples; and (4) modest contamination of the illite standard by small amounts of quartz. Given these caveats and the inherent problems of analyzing mixtures of highly crystalline minerals (quartz and plagioclase) and randomly oriented phyllosilicates (clay minerals), the bulk-powder data should not be used to characterize abundance of individual clay minerals. Moreover, relative values for quartz, plagioclase, and calcite should not be confused with absolute percentages of the total bulk solids.

Beyond routine semiqualitative assessment of relative mineral abundance, we also used XRD to characterize representative samples of volcanic ash. Because of the variability of crystal content, amorphous glass content, and alteration products in such samples, we simply recorded the intensity and area of representative peaks generated by common minerals (e.g., smectite, illite, chlorite, zeolites, quartz, plagioclase, cristobalite, calcite, amphibole, pyroxene, pyrite, and halite). A final parameter to measure is the ratio of peak areas for (100) quartz (d-value =

F3. Examples of X-ray diffractograms showing diagnostic peaks. p. 35.

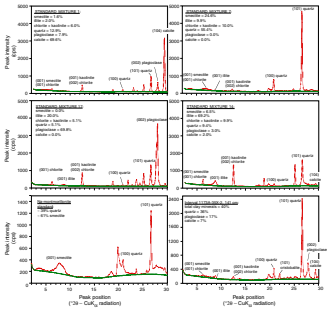

T1. Normalization factors for bulk-powder samples, p. 46.

T2. Measured weight percentages of minerals, p. 47.

T3. Linear regression equations and correlation coefficients in standard mineral mixtures, p. 48.

4.257 Å) to (101) cristobalite (d-value = 4.0397 Å). The accuracy of this ratio suffers from interference between the highest-intensity cristobalite peak and a secondary plagioclase peak at ~22°2θ.

STRUCTURAL GEOLOGY

Our procedures for documenting the structural geology of the Leg 190 cores largely followed those given in the recent account by Kimura, Silver, Blum, et al. (1997), which in turn were based on the approach first developed at Nankai Trough during Leg 131 (Taira, Hill, Firth, et al., 1991). As during all legs, a persistent problem in describing structural features in the cores was the distinction between natural structures and those induced by the drilling process. It was often difficult to decide if a structure was natural, drilling induced, or a natural feature that had been distorted or exaggerated by the drilling process. Core disturbance is not reported here unless we judged that it had some natural significance, and in line with previous legs, we adopted a conservative approach. Also following the practice of previous legs, we were wary of steeply inclined fractures, especially where they lacked strongly and regularly developed slickensides, and we generally considered a feature to be largely of natural origin if it occurred entirely within an intact piece of core.

Each structure observed during Leg 190 was recorded manually on a structural description sheet. Figure **F4** shows the sheet layout that we found useful. One innovation is the column headed "piece interval" for recording the length of the single intact piece of core in which a structure was contained. This information was needed during paleomagnetic reorientation (see below). Features such as a horizontal bedding plane have two identical interval depth values, whereas an inclined structure, such as a fault zone, has an interval top and bottom. The thickness of a dipping structure differs from the length of the interval in which it occurs and was therefore documented in a separate column labeled "thickness." We described structures in the cores using the list of deformational structures developed during Legs 131 (Taira, Hill, Firth, et al., 1991), 156 (Shipley, Ogawa, Blum, et al., 1995), and 170 (Kimura, Silver, Blum, et al., 1997), which were in turn based on the recommendations of Lundberg and Moore (1986). For the purposes of the visual core description forms, the structural identifiers were converted to the symbols listed in Figure **F2.**

F4. Layout of the structural description sheet, p. 36.

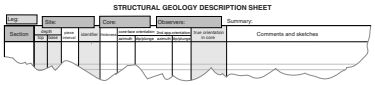

Orientations of structural features were measured using the well-established protractor-goniometer method pictured in Figure **F5** and explained in detail in the "Explanatory Notes" chapter of the Leg 131 *Initial Reports* volume (Shipboard Scientific Party, 1991). For a linear feature, such as sometimes seen on breakage surfaces within the core, a direct measurement of plunge and trend was usually possible, though it was often more convenient in practice to measure the orientation of a toothpick inserted into the core and aligned with the linear structure. In most instances, determining the orientation of planar structures required the measurement of two apparent dips, one being the intersection of the plane with the core face and the other some second intersection, commonly that seen in a surface cut perpendicular to the core face. Again, it was helpful in practice to measure the orientation of a toothpick inserted in line with this second intersection. The two apparent measurements were recorded in columns 7–10 of the structural description sheet (Fig. **F4**). The true spatial orientation was then derived

F5. Protractor-goniometer used for measuring orientations of structures in the cores, p. 37.

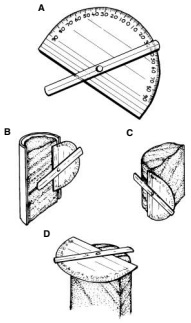

on a stereographic projection program by finding the unique great circle that includes the two apparent dips. The derived value was added to the "true orientation in core" column on the description sheet.

This explicit reference to orientation within the core is necessary because the actual geographic orientation of most cores is not known, having been broken into pieces and differentially rotated during drilling. The core reference system we adopted was as follows. The length of the core was taken to represent vertical; hence, the direction at right-angles to the core axis was the horizontal, to which dip angles and plunges were referred (Fig. F6). The conventions for measuring azimuths have varied during previous legs. In some cases, probably because observations were being made chiefly on the archive half, the 000° azimuth was assigned to the back of that half of the core. Because we found it fruitful to deal with the structures on both the archive and working halves and convenient to be in line with paleomagnetic convention, we referred all structural data to a 000° core azimuth toward the double line at the back of the working half of the core. The back of the archive half was therefore the 180° azimuth.

F6. Core reference system used during Leg 190, p. 38.

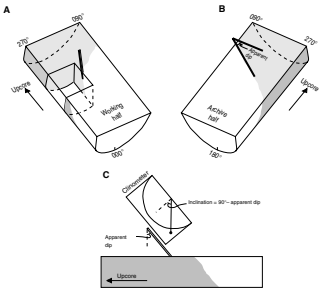

All the numerical data and some commentary were extracted from the description sheets and entered into separate spreadsheets that are included as tables in each site chapter. From this structural database, information was extracted as necessary for statistical manipulation and to produce the various graphical representations of the structural geology presented in the site summaries. We put particular importance on attempting to restore the orientations of structures in the cores to their natural dispositions before drilling.

This further rotation, to true vertical and true north in the geographic reference frame, was remarkably successful during Leg 190. We made some use of the Tensor orientation tool but most of the reorientations were completed using natural remanent magnetization (NRM). The Tensor tool is routinely run with APC cores and provides a compass measurement relating declination from true north to the orientation of the double line on the core liner. Therefore, for APC cores, measured attitudes were reoriented to true geographic coordinates by adding the angle between core reference frame 000° (the double line ruled on the core liner) and true north to the azimuth in the structural measurement.

Because XCB and RCB drilling involve individual core segments differentially rotating, knowing the core liner orientation is not enough to restore the orientations. Instead, NRM declination data were used to reorient the individual pieces of core. We based our procedure on that detailed in Shipboard Scientific Party (1991, p. 44, table 6). However, rather than having to pass individual pieces of core through the cryogenic magnetometer specifically for this purpose, we made use of the routine data that are now readily accessible in the Janus database (see **"Paleomagnetism,"** p. 10).

We had already recorded the interval of an intact segment of rotated core (or several adjacent and clearly similarly oriented pieces) in which a structure of interest occurs as a "piece interval" on the structural description sheet (see above and Fig. F4). We then consulted the Janus paleomagnetic database to find the relevant points at which NRM declination measurements had been made as part of routine paleomagnetic procedures. Two or more determinations per piece are needed to give reliable results, and because the routine measurements are made 5 cm apart, this means that viable segments must be at least ~7 cm in length. Moreover, we considered as suitable only those pieces in which

the paleomagnetic declinations were reasonably consistent: normally that was a difference <10°. A check on the integrity of this procedure was performed on several APC cores by making both Tensor and NRM corrections on the same structural data; the results were found to be very consistent, always agreeing within 10° and in most cases differing by less than 2°. The relevant NRM value extracted from Janus was entered into our structural spreadsheet. We added a simple algorithm based on the steps given in Shipboard Scientific Party (1991, p. 44, table 6) into the spreadsheet so that once the NRM declination had been entered, the true geographic orientation of the structure in question was automatically calculated and stored.

In line with the leg's focus on deformation and fluid flow, a permeameter was brought and operated by the shipboard structural group. The digital gas-probe permeameter, loaned by the Rock Deformation Research group of the University of Leeds, introduces compressed nitrogen at a constant mass rate through an injection tip pressed against the surface of a sample (Fig. **F7**). The measured mass flow rate is recorded by the computer and, at the ambient temperature and pressure, converted to a gas permeability. Although the instrument is designed primarily for the rapid evaluation of dry, coarse clastic sediments, pilot studies showed that systematic patterns were obtainable on water-saturated medium- to fine-grained sediments. While aboard ship, we found that although the geometry and physics of the nitrogen flow were unknown, reproducible but uncalibrated permeabilities were readily obtainable, including values down to 10^{-17} m^2 and less. Therefore, with the ability of the instrument to rapidly obtain large numbers of closely spaced measurements along the cores, the permeameter was able to give a valuable reconnaissance view of the likely fluid flow behavior of the core materials at unprecedented resolution for ODP. However, it is unknown how the reported absolute values relate to true permeability.

A gas pressure of about 100 kPa sealed a soft neoprene disc against the split core face. Sediments below about 100 mbsf were stiff enough to withstand this sealing pressure without undue disturbance, and some measurements were possible on material from as shallow as 7 mbsf. Nitrogen was introduced through a 5-mm central hole in the disc, typically at pressures of a few tens of kilopascals or less in order to avoid internal disturbance to the sediment fabric. Equilibrium flow was usually established in a matter of seconds for coarser, more permeable sediments and after some minutes for materials at the lower part of the instrument's range. The software that accompanies the permeameter is designed for oilfield work and required some modification for ODP use, and the nature of the structure or lithology being probed had to be recorded manually. The computer-stored variables and calculated gas permeabilities were exported to an Excel spreadsheet and combined with the drilling depth information obtained from the ODP database in order to derive plots of the variation of apparent gas permeabilities with downhole depths. Although the permeability values, being based on nitrogen injection into a partially saturated medium, are at best semiquantitative, eventual laboratory-based "back-calibration" may lead to quantitative values and a detailed portrait of the influence of deformation structures and fine lithologic variations on the drainage of the prism sediments.

F7. The gas permeameter used during Leg 190, p. 39.

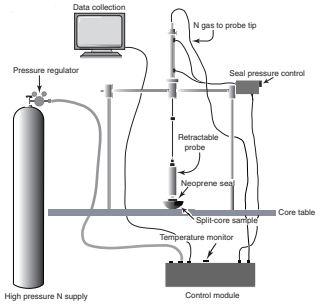

BIOSTRATIGRAPHY

Only one microfossil group, calcareous nannofossils, was examined for biostratigraphic purposes during Leg 190. The goal of the nannofossil analysis was to provide a high-resolution biostratigraphy of sediments in the Nankai Trough. To obtain more detailed records, biostratigraphic zonal assignments during Leg 190 were made on a number of samples within each core (one sample per section).

Methods

Preparation of smear slides for light microscope examination followed standard procedures. Taxon identification was made under plane-, cross-polarized light, and phase contrast using a Zeiss Axioscope microscope at 1000× magnification. Abundance, preservation, and zonal data for each sample investigated were recorded in the Janus paleontology database.

The following scale was used to estimate the relative abundances of individual species. Estimates of percentage of calcareous nannofossils present in each sample were as follows:

B = barren, none.
R = rare, <0.1%.
F = few, from 0.1% to <1%.
C = common, from 1% to <10%.
A = abundant, from 10% to 50%.
D = dominant, >50%.

The assessments of preservation of calcareous nannofossils were based on the following criteria:

P = poor, severe dissolution, fragmentation and/or overgrowth has occurred; primary features may have been destroyed and many specimens can not be identified at the species level.
M = moderate, dissolution and/or overgrowth are evident; besides frequently broken nannofossils, the number of delicate forms is reduced.
G = good, there is little or no evidence of dissolution and/or overgrowth; diagnostic characteristics are preserved and nearly all species (~95%) can be identified.
VG= very good, there is no evidence of dissolution and/or overgrowth; diagnostic characteristics are preserved and all specimens can be identified.

The calcareous nannofossil zonation used here (Fig. **F8**) is that of Martini (1971). Zonal modifications adopted are those proposed by Young (1998). For the Pleistocene, the zonation scheme of Gartner (1977) is employed to provide a higher resolution. Biostratigraphic event zonal markers for the Cenozoic are shown in Figure **F8,** with the events defining the zonal boundaries. In Table **T4,** well-dated nannofossil datums used during Leg 190 are listed.

F8. Biostratigraphic event zonal markers, p. 40.

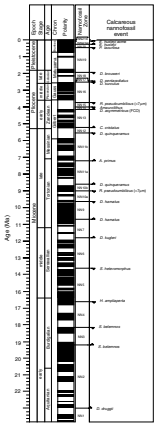

T4. Important calcareous nannofossil datums, p. 49.

PALEOMAGNETISM

Introduction

Paleomagnetic investigations conducted during Leg 190 consisted of measurements of NRM, remanent magnetization after alternating-field (AF) demagnetization of the archive half of core, thermal demagnetization of discrete samples, and acquisition of isothermal remanent magnetization (IRM) of discrete samples. One or two oriented discrete samples were routinely collected from each section of the working half of the core primarily for shore-based analysis of the anisotropy of magnetic susceptibility. For a detailed analysis of the paleomagnetic directions at the boundaries between normal and reversed polarities, paleomagnetic measurements of selected discrete samples were also conducted. The results of these measurements were used to study the magnetostratigraphy and to investigate the magnetic mineralogy of the recovered sections.

To understand core disturbance during APC coring, we conducted an experiment to compare the NRM of whole-round, working-half, and archive-half cores.

Paleomagnetic Instruments

A 2-G Enterprises pass-through cryogenic magnetometer (Model 760R) equipped with direct current superconducting quantum interference devices was used to make the majority of paleomagnetic measurements during Leg 190. This magnetometer is equipped with an in-line AF demagnetizer (2-G Model 2G600) that allows for demagnetization of samples up to 80 mT. The magnetometer and AF demagnetizer are interfaced to a PC-compatible computer and are controlled by the 2-G Long Core software program by National Instruments. A Molspin spinner magnetometer is also available on the ship. Additional instruments used for the demagnetization of samples include a Schonstedt AF demagnetizer (Model GSD-1) capable of demagnetization up to 100 mT and a Schonstedt thermal demagnetizer (Model TSD-1) capable of demagnetization up to 700°C.

Magnetic susceptibility was measured for all whole-core sections with the MST (see **"Physical Properties,"** p. 19). The susceptibility values are stored in the Janus database as raw data in units of 10^{-5} SI. The true susceptibility volumes can be obtained by multiplying the raw data by a correction factor. The standard correction factor for ODP cores is ~0.67 (= 1/1.5).

To investigate the magnetic mineralogy of discrete samples, IRM experiments were conducted using an Analysis Services Company impulse magnetizer (Model IM-10) capable of applying magnetic fields from 0.02 to 1.35 T.

Paleomagnetic Measurements

ODP core orientation designates the positive x-axis direction as the horizontal direction ("geomagnetic north" in a global coordinate reference frame) from the center of the core to the median line between a pair of lines inscribed lengthwise on the working half of each core liner (Fig. **F9**). Continuous NRM and remanence measurements were made on the archive half of each core using the pass-through cryogenic mag-

F9. Paleomagnetic coordinate systems of ODP cores and discrete samples. p. 41.

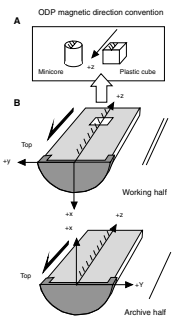

netometer. Remanence measurements were usually made at demagnetization steps of 10, 20, and 30 mT at intervals of 5 to 10 cm.

Paleomagnetic measurements of selected discrete samples were also conducted to gain a better understanding of magnetic polarity boundaries observed in the archive-half cores. Samples were usually demagnetized from 5 to 50 mT, using 5-mT steps. If high magnetic intensity was still observed after the demagnetization of 50 mT, the maximum demagnetization level was increased to 80 mT.

Rock Magnetic Experiments

To investigate the saturation of isothermal remanent magnetization (sIRM) of sediments, 12 IRM steps from 50 to 1300 mT were applied to selected discrete samples. Each sample was then demagnetized at 60 mT after the sIRM measurements. For detailed investigation of magnetic carrier in a sediment, demagnetization of multicomponent isothermal remanent magnetization (mIRM) (Lowrie, 1990) was conducted. For these experiments, orthogonally applied fields of 1.0, 0.3, and 0.1 T were used to generate the IRM components. The samples were then demagnetized using 15 thermal steps from 50° to 650°C.

Discrete Sample Acquisition

One to two discrete oriented samples were acquired from each section of the working half of the core. Paleomagnetic cubes (8 cm^3) were used for removal of soft sediments, whereas minicores were cut from sections of sedimentary and crystalline rock.

Core Orientation

Core orientation of APC cores was achieved with a Tensor tool mounted on the core barrel. Inside the Tensor tool are a three-component fluxgate magnetometer and a three-component accelerometer that record hole inclination (drift), azimuth, and magnetic tool-face readings. For the upper part of the sediments (~30 m), orientation is not usually attempted until the bottom-hole assembly is sufficiently stabilized in the sediment.

Magnetostratigraphy

The Cande and Kent (1995) revised magnetic polarity time scale was used when interpreting magnetic polarity records observed in the core (Fig. **F10**).

F10. Magnetostratigraphic timetable used during Leg 190, p. 42.

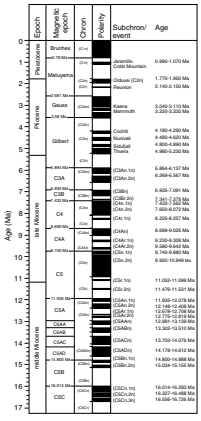

INORGANIC GEOCHEMISTRY

Interstitial Water Sampling and Chemical Analyses

Shipboard interstitial water analyses were performed on 10- to 40-cm-long whole-round sections that were cut and capped immediately after the core arrived on deck. The whole-round samples were usually taken from the bottom of sections of every core that had sufficient recovery, at greater frequency in the top five cores, and across horizons of special interest. Interstitial waters were retrieved by applying the minimum pressure necessary to the sediment and gradually increasing up to

an internal maximum pressure of the squeezer, calculated from the pressure of the press and the ratio of the piston areas of the press and squeezer, of 68 Mpa (10,000 psi) (Manheim and Sayles, 1974). Before squeezing, the sediment was immediately extruded from the whole-round core liner, the surface was carefully scraped to remove potentially contaminated exteriors, and the cleaned sediment was placed into a titanium squeezer on top of a filter that had been previously rinsed in high-purity water. Interstitial water was collected through the filter into a plastic syringe attached to the bottom of the squeezer assembly then filtered through a 0.45-µm polycarbonate filter. Samples were stored in plastic vials pending shipboard analyses. Aliquots for future shore-based analyses were placed in acid-washed plastic tubes and heat-sealed glass ampules.

Interstitial water samples were routinely analyzed for salinity as total dissolved solutes with a Goldberg optical handheld refractometer (Reichart); for pH and alkalinity by Gran titration with a Brinkmann pH electrode and a Metrohm autotitrator; for dissolved chloride, calcium, and magnesium concentrations by titration; and for silica, phosphate, and ammonium by spectrophotometric methods with a Milton Roy Spectronic 301 spectrophotometer, following the analytical techniques described by Gieskes, et al. (1991). International Association of Physical Sciences Organizations (IAPSO) standard seawater was used for calibrating most techniques. The reproducibility of these analyses, expressed as 1-σ standard deviations of means of multiple determinations of IAPSO standard seawater or of a standard, are alkalinity, <1.5%; chloride, <0.2%; calcium, <0.5%; magnesium, <0.5%; silica, <3%; and phosphate and ammonium, 4%. At all sites, sodium was determined using charge balance calculations where $\Sigma_{(\text{cation charge})} = \Sigma_{(\text{anion charge})}$.

Potassium and sulfate were analyzed by ion chromatography (IC) using the Dionex DX-100. The reproducibility of these analyses expressed as 1-σ standard deviations of means of multiple determinations of IAPSO standard seawater are potassium, <2%, and sulfate, ~1%. Calcium and magnesium were also routinely determined using IC, but for most analyses the titration data are reported except where specifically noted; the titration method for calcium and magnesium provided more accurate and precise results. For calcium, a precision of ~2% (1-σ standard deviation of repeat IAPSO determinations/published IAPSO concentration) of IAPSO standards was obtained by IC as opposed to <0.5% by titration. For magnesium, the precision was low (~5% by IC) and also compared unfavorably with <0.5% relative error by titration. Although the IC method is not optimized for the high concentrations of sodium and chloride found in marine interstitial waters relative to the concentrations of the other constituents, they were routinely analyzed with the other cations and anions, respectively. Even for sodium and chloride the precision by IC is ~1% for Cl and <2% for Na; however, the accuracy is very low. These IC results, however, provided a useful check on the general trends of the depth profiles.

Chemical data for interstitial waters are reported in molar units.

Hydrogen Analysis

Hydrogen concentrations of interstitial waters were determined on ~5-cm^3 bulk-sediment samples that were collected immediately after the core arrived on deck. Whole-round sediment samples were first transferred into an anaerobic glove box and then subsamples were transferred into 20-mL headspace vials. Care was taken to avoid sedi-

ment that had been contaminated during drilling or handling. In soft sediments, this involved sampling interior material with a cut off syringe, whereas in harder materials, the outer disrupted parts of the core were pared off. Following the placement of the sediment sample in the headspace vial and removal of the vial from the glove bag, the headspace was flushed with oxygen-free and hydrogen-free nitrogen. The vials were then incubated at in situ temperatures and analyzed for hydrogen over a period of a few days. Individual subsamples were prepared in replicate. Replicate samples were autoclaved prior to incubation in order to quantify abiogenic hydrogen. A trace analytical reduction gas analyzer was used to determine headspace hydrogen concentrations.

In Situ Interstitial Water

The water sampling temperature probe tool (WSTP) (Barnes, 1988) was used for sampling bottom seawater at Sites 1173 and 1175 and for in situ extraction of interstitial water. The tool is lowered on the coring wire to the end of the drill string, where it hooks onto an assembly just above the bit with the probe tip extruding below the bit. The bit was lowered either into bottom water, ~50 m above mudline without pumping to avoid mixing surface water (drill water) with bottom seawater, or into the bottom with the filter assembly projecting ~1.1 m past the bit. A time-operated valve opens and interstitial water is drawn under negative pressure through the filter and into the sampler. The filter assembly is 22 cm long and its surface area is 200 cm^2.

Prior to deployment, the fluid path is backfilled with distilled water that has been previously degassed by nitrogen bubbling. The overflow cylinder is flushed with nitrogen and evacuated. A timer is set for a fixed time after which the valve opens, exposing the sampling line and chamber to ambient pressure. The timer also closes the valve after a prearranged time interval of 5–15 min.

Fluid from the titanium and stainless steel coils was filtered (through a 0.45-µm filter) and analyzed following the procedures described for the interstitial water squeezed from whole-round samples.

Inorganic Carbon

Inorganic carbon was determined using a Coulometrics 5011 carbon dioxide coulometer equipped with a System 140 carbonate carbon analyzer. A known mass (40–50 mg) of freeze-dried (dedicated carbonate samples) or oven-dried (physical properties samples) ground sediment was reacted in a 2-N HCl solution. The liberated CO_2 was titrated in a monoethanolamine solution with a colorimetric indicator, and the change in light transmittance was monitored with a photodetection cell. The percentage of carbonate was calculated from the inorganic carbon content assuming that all carbonate is present as calcium carbonate:

$$\%CaCO_3 = \%C_{inorg} \times 100/12.$$

The precision of these analyses, expressed as 1-σ standard deviations of means of multiple determinations of a pure carbonate standard is <1%.

Elemental Analysis

Total nitrogen, carbon, and sulfur of sediment samples were determined using a Carlo Erba Model NA 1500 NCS analyzer. Mixtures of vanadium pentoxide and crushed, freeze-dried samples (~5 mg) were combusted in an oxygen atmosphere at 1000°C, converting total (organic and inorganic) carbon to CO_2, sulfur to SO_2, and nitrogen to NO_2. The NO_2 was then reduced to N_2 using copper. The gases were separated by gas chromatography and measured with a thermal conductivity detector. The precision of these analyses, expressed as 1 standard deviation, is 2%–3%. Total organic carbon (TOC) was determined by calculating the difference between total carbon (TC) from the NCS analyzer and inorganic carbon from the coulometer:

$$TOC = TC - C_{inorg}.$$

ORGANIC GEOCHEMISTRY

The shipboard organic geochemistry program for Leg 190 included (1) real-time monitoring of volatile hydrocarbons as required by ODP safety regulations, (2) measurement of the inorganic carbon and carbonate content of the sediments, and (3) elemental analyses of total nitrogen, sulfur, and carbon. All methods and instruments used during Leg 190 are described in detail by Kvenvolden (1985), Claypool and Kvenvolden (1983), and in the "Explanatory Notes" chapter of the Leg 156 *Initial Reports* volume (Shipboard Scientific Party, 1995).

Volatile Hydrocarbons

For safety and pollution prevention, concentrations and distributions of light hydrocarbon gases, mainly methane, ethane, and propane, were monitored for each core following standard headspace sampling. Briefly, 5-cm³ sediment samples were collected using a calibrated borer tool while the core was still on deck. The samples were placed in 20-mL glass serum vials and sealed with a septum and metal crimp cap. When consolidated or lithified samples were encountered, chips of material were placed in the vial and sealed. Before gas analyses, vials were heated to 60ºC for 30 min. A 5-cm³ subsample of the headspace gas was extracted from each vial using a standard glass syringe for gas chromatograph (GC) analysis. When gas pockets were encountered, vacutainer samples were collected by piercing the core liner using a syringe connected to a penetration tool.

The constituents of the gas were analyzed using an HP5890 Series II GC equipped with a 0.32 cm × 2.4 m stainless steel column filled with HayeSep R porous polymer packing (80/100 mesh). When heavier molecular-weight hydrocarbons (C_3 and higher) were detected, the sample was analyzed by a natural gas analyzer, which quantifies C_1 to C_6, nitrogen, oxygen, and carbon dioxide concentrations. Helium was used as the carrier gas. Data acquisition and processing was performed using HP Chemstation software. Chromatographic response was calibrated against authentic standards, and the results are reported in parts per million by volume (ppmv).

Inorganic Carbon

Inorganic carbon (IC) was determined using a Coulometrics 5011 carbon dioxide coulometer equipped with a System 140 carbonate carbon analyzer. Samples of 10–12 mg of freeze-dried, ground sediment were weighed and reacted with 2-M HCl to liberate CO_2. The CO_2 was titrated and the change in light transmittance monitored by a photodetection cell. The weight percentage of calcium carbonate was calculated from the IC content, assuming that all the evolved CO_2 was derived from dissolution of calcium carbonate, using the following equation:

$$CaCO_3 = IC \times 8.33.$$

The amount of carbonate is expressed as weight percent, assuming all the carbonate was present as calcite. No correction was made for other carbonate minerals.

Elemental Analysis

TC, nitrogen, and sulfur were analyzed using a Carlo Erba 1500 CNS Analyzer. An aliquot of 12–15 mg freeze-dried, ground sediment combined with V_2O_5 catalyst was combusted at 1000°C in a stream of oxygen. Nitrogen oxides were reduced to N_2. The mixture of N_2, CO_2, and SO_2 gases was separated by a GC equipped with a thermal conductivity detector. All measurements were calibrated by comparison to synthetic standards. The amount of TOC in weight percent was calculated as the difference between TC in weight percent and IC in weight percent by the following equation:

$$TOC = TC - IC.$$

MICROBIOLOGY

Bacteria play a dominant role in the degradation of organic matter within sediments, and as a consequence, drive chemical changes and early diagenesis. The existence of a deep bacterial biosphere in marine sediments has only recently been established (Parkes et al., 1994), but already the activity of bacteria in depths to 750 mbsf and their direct involvement in geochemical changes have been demonstrated.

Little is understood about what types of bacteria are found deep below the seafloor, what they use for energy and carbon sources and the rate of their activity, how healthy the population is, and how much they affect the environment around them. For example, recent research (Wellsbury et al., 1997) has shown that temperature increases during burial can result in organic matter becoming easier to degrade by bacteria and that bacterial populations and activity can increase in deeper layers below 100 mbsf. Increasing organic matter bioavailability was reflected by increases of up to a thousandfold in substrates for bacterial activity (volatile fatty acids, particularly acetate) in deep sediments (Leg 164; Paull, Matsumoto, Wallace, et al., 1996). Thus, bacterial populations may exist at much greater depths and may even increase with depth, rather than decrease as energy sources "improve" with increasing depth and temperature.

The work undertaken during Leg 190 will identify the bacterial mechanisms important in the environment and determine the impact these have on sediment geochemistry. This investigation has been designed to address the following questions: (1) can we improve methods of culturing deep-sediment bacteria (e.g., sulfate reducers, iron reducers, and oxidizers) and obtain more useful viable counts, and can we isolate new organisms; (2) how many bacteria are present in very deep subsurface sediments, and can we determine when a bacterial cell has died; (3) are there increasing concentrations of labile organic carbon (acetate) with depth, and what affect would this increase have on rates of methanogenesis measured at in situ temperatures and pressures; and (4) using molecular genetics, can we identify and characterize the bacterial populations deep in the sediments, and what biomarkers are present and currently being produced? Leg 190 also provided the deepest samples yet collected for bacterial analyses.

Microbiology samples consisted of plug minicores of a few cubic centimeters from whole-round cores (WRCs), IW splits, and split core samples from the sample table.

Plugs

Sediment in 1-cm^3 plugs was taken for shipboard direct microscopic determination of bacterial numbers. These plugs were taken from the end of selected 1.5-m core sections immediately after the sections were cut on the catwalk and before they were sealed with an end cap. Potentially contaminated sediment was removed with a sterile scalpel, and a sterile 5-cm^3 plastic syringe with the luer end removed was used to take a 1-cm^3 plug. The syringe was sealed with a sterile Suba-Seal stopper. In a clean area of the laboratory, the 1-cm^3 plug was extruded into a sterile serum vial containing 9 mL of filter-sterilized (0.2 µm) 4% formaldehyde in 3.5% NaCl. The vial was crimped and shaken vigorously to disperse the sediment particles.

Whole-Round Core Samples

WRCs were cut from 3.0-m (double) core sections on which the end caps had not been sealed with acetone. The double core sections were removed from the catwalk and brought into the core reception area, where they were cleaned, wiped with ethanol, and placed into a sterile (autoclaved) cutting rig flushed constantly with sterile oxygen-free nitrogen (OFN) to maintain anoxia. The initial cut was made at 1.5 m, and the entire lower section was returned the curator. WRCs of varying lengths were then removed from the base of the retained core section upward. In general, the first WRC was for IW; subsequent WRCs were for microbiology. Each WRC was capped with standard core end caps or sterile (γ-irradiated) core end caps, where appropriate, under OFN. Core end caps were sealed with insulation tape and the whole WRC was either (1) stored at –80°C, (2) stored in gas-tight aluminum/plastic bags in an anoxic atmosphere (Anaerocult-A, Merck) at –80°C, (3) stored in gas-tight aluminum/plastic bags in an anoxic atmosphere at 4°C, or (4) moved to an anaerobic cabinet for initial microbiological handling. The last 5-cm WRC was cut and left uncapped. It was wrapped in sterile aluminum foil and immediately transferred to the anaerobic cabinet for processing.

Interstitial Water Samples

IW splits of as much as 3 mL where possible were taken for shore-based acetate analysis (Wellsbury et al., 1997). When squeezed IW volume was unavailable, 10-cm^3 of a squeeze cake was taken instead. Samples were stored frozen (–20°C).

After alkalinity was measured in the chemistry lab, ~2.0-mL aliquots of the acidified solution were transferred to glass headspace vials and stored at –20°C for dissolved organic carbon analysis.

The acidified IW samples were sparged with CO_2-free air and oxidized on a platinum catalyst at 680°C in a total carbon analyzer (Shimadzu TOC 5000A). The CO_2 produced upon oxidation was quantified using a nondispersive infrared detector.

Split-Core Samples

Sediment samples were removed from the split-core sampling tables for shore-based lipid analysis. One quarter of a WRC, 30 cm in length, was removed from the working half using latex gloves. Samples were individually wrapped in aluminum foil and stored in nonheat-sealed polyethylene bags at –80°C.

Shipboard Laboratory Handling

Acridine Orange Direct Counts

Total bacterial abundance and numbers of dividing/divided cells were determined using acridine orange as a fluorochrome dye with epifluorescence microscopy (Fry, 1988). Fixed samples were mixed thoroughly, and a 5- to 10-µL subsample was added to 10 mL of 2% (by volume) filter-sterilized (0.1 µm) formaldehyde in 3.5% NaCl. Acridine orange (50 µL of a 1-g/L filter-sterilized [0.1 µm] stock solution) was added, and the sample was incubated for 3 min. Stained cells and sediment were trapped on a 0.2-µm black polycarbonate membrane (Osmonics, USA). Excess dye was removed from the membrane by rinsing with a 10-mL aliquot of 2% (v/v) filter-sterilized formaldehyde in 3.5% NaCl. The membrane was mounted for microscopic analysis in a minimum of paraffin oil under a coverslip.

Mounted membranes were viewed under incident illumination with a Zeiss Axiophot microscope fitted with a 50-W mercury vapor lamp, a wide-band interference filter set for blue excitation, a 100× (numerical aperture = 1.3) Plan Neofluar objective lens, and 10× eyepieces. Bacterially shaped fluorescing objects were enumerated, with the numbers of cells on particles doubled in the final calculations to account for masking. Dividing cells (those with a clear invagination) and divided cells (pairs of cells of identical morphology) were also counted.

Cell Viability

Subsamples (5–20 µL) of the slurries were filtered through a 0.22-µm membrane filter (Millipore Corp.). Filters were stained with 100 µL of Live/Dead BacLight Kit for 20 min then dried and mounted with nonfluorescent immersion oil on glass microscope slides and examined with epifluorescence microscopy (420-nm excitation filter; 590-nm barrier filter) at 1000× using an epifluorescent microscope.

Two approaches were used to assess bacterial metabolic activity, fluorescene diacetate (FDA) and 5-cyano-2,3-ditolyl tetrazolium chloride (CTC). Subsamples (5–20 µL) were filtered through a 0.22-µm membrane filter (Millipore Corp.). These were stained with FDA-dimethyl sulfoxide (12-µM final concentration) for 20 min. Filters were dried and mounted with nonfluorescencing immersion oil on glass microscope slides and examined under 1000× magnification. FDA-stained microorganisms were viewed using a 520-nm barrier filter.

Diluted slurries were incubated in triplicate with 5% CTC in sterile test tubes for 4 hr at room temperature. After incubation, selected samples were counterstained with 50 µg/L of the DNA-binding fluorochrome 4′,6-diamidino-2-phenylindole (DAPI) to determine the total cell abundance in the same preparation. Subsamples were filtered (0.22 µm, Millipore Corp) and dried and mounted with nonfluorescent immersion oil on glass microscope slides and examined under 1000× magnification. CTC-treated preparations were viewed using a blue (420 nm) excitation filter used in combination with a 590-nm barrier filter. CTC- and DAPI-stained microorganisms in the same preparation could be viewed simultaneously with a 365-nm excitation filter and a 400-nm cutoff filter.

Enrichment Cultures

A 5-cm WRC was placed in the anaerobic chamber, and 1-cm^3 plugs were taken with sterile syringes to inoculate enrichment cultures. Anaerobic growth media for sulfate-reducing, iron-oxidizing, iron-reducing, and denitrifying bacteria (Widdel and Bak, 1992) were utilized. An additional 2-cm^3 plug was removed for shore-based DNA/RNA analysis. The residue of the WRC was removed from the core liner using a sterile steel spatula, leaving the outer, potentially contaminated sediment adjacent to the core liner. The sediment was stored in plastic bags with an oxygen scrubber at –80°C for shore-based fatty acid analysis.

The uncapped WRC was subsampled in the anaerobic cabinet for viable counts of sulfate-reducing and iron-reducing bacteria. Viable counts were also initiated for *Methanococcus* sp. Additional plugs (3 cm^3) were collected from the WRC using sterile syringes and then placed in plastic tubes and frozen at –80°C for shore-based DNA extraction and analysis. The residue was stored in a plastic ZipLok bag at –80°C for shore-based analysis of nucleic acids.

Contamination Assays

To confirm the suitability of the core material for microbiological research, contamination assays were conducted to quantify the intrusion of drill water using the chemical and particulate tracer techniques described in *ODP Technical Note* 28 (Smith et al., 2000), except that the extraction of the particulate tracer, fluorescent microspheres, has been modified to increase the sensitivity of the assay. The modification consists of suspending the sediment sample in a solution of saturated NaCl. The solution is centrifuged for 5 min (Marathon 10K, 2800 × g), and the supernatant containing the microspheres is filtered through polycarbonate filters (0.2-µm pore size). The microspheres are counted, and data are reported as number of microspheres per gram of sediment.

PHYSICAL PROPERTIES

Introduction

Physical properties were measured on unsplit cores and on the undisturbed parts of split cores. The MST was used for nondestructive measurements of wet bulk density, *P*-wave velocity, magnetic susceptibility, and natural gamma radiation on unsplit cores. Thermal conductivity measurements were also conducted on unsplit sediment cores and split rock cores. Undrained shear strength was measured on unlithified sediment cores, and three-directional *P*-wave velocities were measured on both soft and lithified sediment cores. Portions of split cores that were undisturbed by drilling, sampling, gas expansion, bioturbation, cracking, and large voids were used to obtain specimens for moisture and density measurements and calculations (wet bulk density, grain density, dry bulk density, water content, void ratio, and porosity).

Physical properties measurements were conducted after the cores had equilibrated to near ambient room temperature (i.e., 22°–24°C) after ~2–4 hr. A summary of each of the physical properties measurement procedures for Leg 190 is outlined below; more detailed descriptions are provided by Blum (1997).

Multisensor Track Measurements

The first measurement station was the MST, which combines four sensors on an automated track to measure magnetic susceptibility, bulk density, *P*-wave velocity, and natural gamma-ray emission on whole-core sections. The four MST sensors are the magnetic susceptibility meter, the gamma-ray attenuation (GRA) bulk densiometer, the *P*-wave logger (PWL), and the natural gamma-ray (NGR) detector. Magnetic susceptibility, bulk density, and natural gamma-ray emission were generally measured on all cores indiscriminately of coring method, (i.e., APC, XCB, or RCB). *P*-wave velocities were measured on undisturbed APC cores. MST measurement of *P*-wave velocities on XCB and RCB cores is not usually recommended because there is incomplete coupling between the liner and the core. MST data were sampled at discrete intervals, with the sampling rate chosen to optimize the data resolution and the time needed to run each core section through the device.

Magnetic Susceptibility

Magnetic susceptibility was measured with a Bartington meter MS2 using an 80-mm internal diameter sensor loop (88-mm coil diameter) operating at a frequency of 565 Hz and an alternating field of 80 A/m (0.1 mT). The sensitivity range was set to the low sensitivity setting (1.0 Hz). The sample period and interval were set to 2 s and 4 cm, respectively, unless noted otherwise. The mean raw value of the measurements was calculated and stored automatically. The quality of these results degrades in XCB and RCB cores, where the core may be undersized and/or disturbed. Nevertheless, general downhole trends are useful for stratigraphic correlations. The MS2 meter measures relative susceptibilities, which have not been corrected for the differences between core and coil diameters.

Gamma-Ray Attenuation

Bulk density was estimated for unsplit core sections as they passed through the GRA bulk densiometer using sampling periods and intervals of 2 s and 4 cm, respectively, unless noted otherwise. The gamma-ray source was ^{137}Cs. For each site, the GRA bulk densities and the bulk densities measured on discrete samples were compared.

P-Wave Velocity

P-wave velocity was measured at 4-cm intervals and 2-s periods with the high-resolution PWL. The PWL measured *P*-wave velocity across the unsplit core sections. In order to determine the *P*-wave velocity, the PWL transmits 500-kHz *P*-wave pulses through the core at a frequency of 1 kHz. The transmitting and receiving transducers are aligned perpendicular to the core axis while a pair of displacement transducers monitors the separation between the *P*-wave transducers. Variations in the outer diameter of the liner do not degrade the accuracy of the velocities, but the unconsolidated sediment or rock core must completely fill the liner for the PWL to provide accurate results.

Natural Gamma-Ray Emissions

Natural gamma-ray emission analysis is a function of the random and discrete decay of radioactive atoms and is measured through scintillating detectors as outlined by Hoppie et al. (1994). During Leg 190, NGR was measured for 20 s for each 20-cm length of core unless noted otherwise. NGR calibration was performed at the beginning of the leg, and sample standards were measured at the end of every site.

Thermal Conductivity

Unconsolidated sediment and rock samples were measured for thermal conductivity in the shipboard laboratory using the TK04 system described by Blum (1997). This system employs a single-needle probe (von Herzen and Maxwell, 1959) heated continuously, in "full-space configuration" for soft sediments and in "half-space configuration" for lithified sediments. Under conditions of moderate to full recovery, thermal conductivity measurements were conducted at a frequency of two per core.

Thermal conductivity was measured on unsplit-core unconsolidated sediment sections using a full-space single-needle probe TeKa (Berlin) TK04 unit. A hole was drilled in the outer core liner, and the 2-mm-diameter temperature probe was inserted into the working half of the core section. For lithified samples, a smooth surface was prepared on ~5-cm-long split-core specimens that had been placed in a water bath for a minimum of 15 min. The half-space needle probe was secured onto the flat surface of the half core. At the beginning of each half- and full-space measurement, temperatures in the samples were monitored automatically, without applying a heater current, until the background thermal drift was determined to be <0.04°C/min. The heater circuit was then closed and the temperature increase in the probe was recorded.

The reported thermal conductivity measurement for each sample is the average of three and four repeated measurements for the full- and half-space methods, respectively. Data are reported in W/(m·°C) with a stated error of ~5%. The choice of measurement interval and assess-

ment of thermal stability are automatic with the TK04 meter, which does not require shipboard calibration.

Moisture and Density Measurements

Moisture and density (MAD) measurements were determined by measuring wet mass, dry mass, and dry volume of specimens from split cores. Samples were collected at a frequency of two per section. Where a whole-round sample was taken from a section, one of the two MAD samples was taken adjacent to it. Care was taken to sample undisturbed parts of the core and to avoid drilling slurry.

Immediately after the samples were collected, wet sediment mass (M_{wet}) was measured. Dry sediment mass (M_{dry}) and dry sediment volume (V_{dry}) were determined after the samples had dried in a convection oven for 24 hr at a temperature of 105° ± 5°C. Wet and dry masses were determined using electronic balances, which compensated for the ship's motion, and dry volume was measured using a gas pycnometer.

Moisture content, grain density, bulk density, and porosity were calculated from the measured wet mass, dry mass, and dry volume as described by Blum (1997). Corrections were made for the mass and volume of evaporated seawater using a seawater density of 1.024 g/cm^3 and a salt density of 2.20 g/cm^3.

P-wave Velocities on Split Cores

The method chosen for *P*-wave velocity measurements (V_P) was dependent on the degree of sediment consolidation. For unconsolidated sediments, the *P*-wave sensors 1 and 2 (PWS1 and PWS2) insertion probe system was used to measure the transverse and longitudinal (i.e., along the core axis) *P*-wave velocity. In semilithified sediments, only the modified Hamilton frame velocimeter (PWS3) contact probe system, described by Boyce (1976), could be employed. Where sediments were sufficiently indurated for cutting with a saw, velocity measurements were made on ~8-cm^3 oriented cubes. If core recovery permitted, two to three velocity measurements were conducted per core.

The PWS1 and PWS2 probe system calculates *P*-wave velocity based on a fixed distance and measured traveltime. Anisotropy was calculated by the following equation:

$$\text{Anisotropy (\%)} = (V_{Pt} - V_{Pl})/[(V_{Pt} + V_{Pl})/2] \times 100,$$

where V_{Pt} is the transverse *P*-wave velocity and V_{Pl} is the longitudinal velocity. The velocity meter was calibrated by measuring V_P in water.

In addition to traveltime, the PWS3 system measures sample thickness with a digital micrometer. Measurements were generally taken two to three times per core, with more measurements taken in sections characterized by varying lithology. In cores that were too consolidated for the PWS1 and PWS2 insertion probes but too soft or friable to cut into cubes, the PWS3 system was used to measure *P*-wave velocity in the x-direction. In hard rock, cubes were oriented, cut, and then rotated so that the PWS3 system could measure velocities in the x-, y-, and z-directions.

Electrical Conductivity

Electrical conductivity was measured with two different methods, both using the Wayne-Kerr component analyzer in the 10-KHz to 30-kHz range. With samples saturated with saline pore water, polarization effects are minimal in this frequency range, and the measured conductivity is largely independent of frequency. In soft sediment cores (APC cores), a Wenner needle array was used. Four electrodes 1 cm long and spaced ~1 cm apart were inserted into the working half. The two outer electrodes inject an alternating current while the two inner electrodes measure the resulting potential difference. The apparent resistance (R) is inversely proportional to the conductivity of the medium. Calibration was performed after each measurement by immersion of the electrode array in seawater. The conductivity of seawater (c_w) as a function of temperature is computed from the formula

$$c_w = (2.8\ \text{S/m} + 0.1\ \text{S/m/°C}).$$

The formation factor is then

$$F = R_{core}/R_{calibration} - c_w(T_{calibration})/c_w(T_{core}).$$

This definition of the formation factor does not take into account surface conductivity effects but is convenient for correction of temperature effects and for comparison with porosity data. Ambient temperature ranged from 23° to 28°C, and the temperature difference between core temperature and calibration temperature was usually <2°C. Measurements were performed both along and across the core axis and often yielded an anisotropy of a few percent. This anisotropy may be caused at least in part by cracking perpendicular to the core axis and was not reported on the graph. When the cores were lithified enough to cut cubic samples, cubes were placed between two stainless steel electrodes, and impedance, which is a complex number, was measured with the Wayne-Kerr component analyzer. To assure good contact between sample and electrodes, filter papers were thoroughly soaked in seawater and care was taken to avoid trapped gas bubbles and to remove excess water dripping on the sides of the sample. Residual contact impedance was obtained from measurements of two seawater-saturated filter papers with no sample.

For correction, the contact impedance was subtracted from the impedance measured on samples. The nonreal part of the complex impedance was small and was generally accounted for by the contact impedance. Sample conductivity (c_{11}) was computed from the three dimensions of the cube (L_1 = length between the electrodes, and L_2 and L_3 = lengths in the other directions) and from the real impedance (R) as

$$c_{11} = (L_1/R)L_2L_3.$$

Sample dimensions were obtained with the PWS3 system during *P*-wave velocity measurements. Measurements in all three directions (c_{xx}, c_{yy}, and c_{zz}) were performed when possible. Horizontal and vertical electrical conductivity anisotropy are defined as for the *P*-wave velocity anisotropy:

$$\text{Anisotropy}_h\ (\%) = 200\ (c_{xx} - c_{yy})/(c_{xx} + c_{yy}),\ \text{and}$$

$$\text{Anisotropy}_v\ (\%) = 200\left(\frac{c_{xx}}{2}+\frac{c_{yy}}{2}-c_{zz}\right)/\left(\frac{c_{xx}}{2}+\frac{c_{yy}}{2}+c_{zz}\right)$$

The formation factor in each direction is computed as

$$F_i = c_{ii}/c_w,$$

where c_w varies with temperature as described above.

Shear Strength

Undrained shear strength (S_u) was measured using a motorized miniature vane shear apparatus that was inserted into soft sediment and rotated until the sediment failed, following the ASTM D4648-87 procedure (ASTM, 1989). The difference in rotational strain between the top and bottom of the vane shear spring was measured digitally, and the peak shear strength was recorded. Shear strength measurements by this apparatus are reliable to a threshold of 100–150 kPa.

DOWNHOLE MEASUREMENTS

Introduction

Well logging provides continuous, in situ records of geophysical parameters within a borehole. These measurements are used to assess the physical, chemical, and structural characteristics of formations penetrated by drilling and thus provide a means of reconstructing and interpreting geological environments. During Leg 190, wireline logging was performed only at Site 1173. Other sites were not logged because logging while drilling (LWD) is planned for all of these sites during Leg 196 in 2001. Of particular interest during Leg 190 was the collection of log sonic velocity information, as currently available LWD technology does not permit the collection of velocity logs necessary both to tie seismic velocities to borehole depth with accuracy and to document sediment elastic properties.

Downhole logging operations begin after the hole has been cored and flushed with a viscous drilling fluid. The drilling assembly is then pulled up to ~80 mbsf, and the logging tools are passed through the drill pipe into the open hole. The logging tools are joined together into tool strings so that compatible tools are run together. Each tool string is lowered separately to the base of the hole and then measurements are recorded as the tool string is raised at a constant velocity between 275 and 500 m/hr. A wireline heave compensator is used to minimize the effect of the ship's heave on the tool position in the borehole (Goldberg, 1990).

Tool-String Configurations

Two tool strings were used during Leg 190: the triple combination tool (triple combo), and the Formation MicroScanner-sonic (FMS-sonic) (Fig. **F11;** Tables **T5, T6**). The principles underlying the use of these tools are explained on the Lamont-Doherty Earth Observatory Borehole Research Group's Web site (see the **"Related Leg Data"** contents list) and in Schlumberger Corp. (1989), Serra (1984a, 1984b, 1989), Timur and Toksöz (1985), and Tittman (1986). Some examples of the logging

F11. Leg 190 wireline tool strings, p. 43.

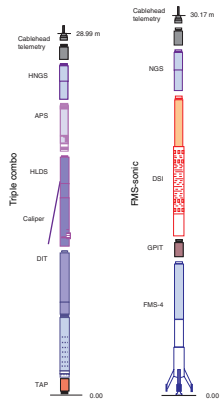

T5. Leg 190 wireline tool strings, p. 50.

T6. Tool-string and measurements acronyms, p. 51.

tools' applications are given by Ellis (1988) and Rider (1996). The following is a summary of the principles of operation of the tools used.

Natural Gamma-Ray Sonde and the Hostile Environment Natural Gamma-Ray Sonde

The natural gamma-ray sonde (NGS) and the hostile environment natural gamma-ray sonde (HNGS) measure the gamma radiation of U, K, and Th, which occur naturally in sediments. Because of the relative abundance of U, Th, and K within many clay minerals, a high gamma-ray reading is often indicative of a relatively high clay content in the sediment, whereas a low gamma-ray reading often indicates quartz sands and carbonates (e.g., Serra and Sulpice, 1975). It should be mentioned, however, that this is not always the case (see Rider, 1990).

A gamma-ray sonde was fitted to all of the tool strings to enable depth correlation between each individual logging run. The data from the HNGS on the triple-combo tool string are used as the reference gamma-ray log because the HNGS produces a more precise measurement than the NGS (Schlumberger, 1994). The natural gamma-ray reading was also used for measuring the depth to the seafloor, as natural gamma-ray radiation shows a sharp increase at the mudline.

Accelerator Porosity Sonde

The accelerator porosity sonde (APS) emits fast neutrons, which lose energy as they collide with hydrogen nuclei in the formation. Once the neutrons have slowed down to reach thermal energies (0.025 eV), they are captured by the nuclei of chlorine and various heavy elements. This results in a gamma-ray emission. The APS measures the number of neutrons arriving at five different detectors at varying distances from the source. This measurement is inversely proportional to the concentration of hydrogen in the formation. Because the majority of hydrogen is contained in the pore water, the APS measurement can be used to derive a porosity. However, hydrogen bound in minerals, such as clays, also contributes to the APS measurement, so that the raw porosity value is often an overestimate. Furthermore, the presence of certain rare earth and trace elements with particularly large capture cross sections (e.g., boron and cadmium) can have a significant effect on the APS reading (Harvey et al., 1996). Because of the high clay content in virtually all Leg 190 sediments, the neutron porosity data were considered to be inaccurate with respect to true porosity (see **"Downhole Measurements,"** p. 30, in the "Site 1173" chapter).

Hostile Environment Lithodensity Sonde

The hostile environment lithodensity sonde (HLDS) consists of a ^{137}Cs radioactive source and two gamma-ray detectors mounted on a shielded sidewall skid that is pressed against the formation by a hydraulically activated arm. The arm also provides a caliper measurement of borehole diameter. The gamma rays emitted by the source interact with the electrons in the formation and lose energy as a result of Compton scattering. When the gamma rays reach a low energy (<150 keV), photoelectric absorption takes place. This tool is sensitive to hole conditions, as the detectors need to be in contact with the borehole wall to produce reliable data.

The number of gamma rays that reach the detectors in the HLDS is directly related to the number of electrons in the formation, which is in turn related to the bulk density. The bulk-density value measured by the HLDS can be used to calculate a porosity using the following equation:

$$\phi = (\rho_{gr} - \rho_b) / (\rho_{gr} - \rho_w),$$

where ρ_{gr} = mean grain density, given by physical properties measurements (typically 2.7 g/cm³); ρ_w = pore water density, taken to be 1.03 g/cm³ for seawater; and ρ_b = bulk density, given by the HLDS.

The photoelectric effect (PEF) can be assessed by comparing the counts from the far detector of the HLDS, which is in the high-energy region where only Compton scattering occurs, with those of the near detector, which is in the low-energy region where the PEF is dominant. Photoelectric absorption is strongly dependent on the atomic number of the constituents of the formation. The PEF values, therefore, can give an indication of the chemical composition of the rock.

Dual Induction Tool

The dual induction tool provides three different measurements of electrical resistivity based on multiple depths of investigation: deep induction, medium induction, and shallow, spherically focused resistivity (SFL). The two induction devices produce an alternating magnetic field, which induces Foucault currents around the borehole. These currents produce a new inductive signal that is proportional to the conductivity of the formation. The measured conductivities are then converted to resistivity (ohm-meter). The SFL measures the current necessary to maintain a constant voltage drop across a fixed interval and is a direct measurement of resistivity. Because the solid constituents of rocks are essentially infinitely resistive relative to the pore fluids, resistivity is controlled mainly by the nature of the pore fluids, porosity, and permeability.

Temperature/Acceleration/Pressure Tool

The temperature/acceleration/pressure tool (TAP) tool uses both fast- and slow-response thermistors to detect borehole fluid temperature at two different rates. The fast-response thermistor is able to detect small abrupt changes in temperature, whereas the slow-response thermistor is used to estimate temperature gradient and thermal regimes more accurately. Data from the TAP tool provide an insight into the thermal regime of the formation penetrated by drilling. A three-axis accelerometer is also used to measure tool movement downhole, which allows the effects of heave to be analyzed.

Dipole Shear Sonic Imager

The dipole shear sonic imager (DSI) employs a combination of monopole and dipole transducers (see Fig. F12) to measure sonic wave propagation in a wide variety of lithologies (Schlumberger Corp., 1995). In addition to robust and high-quality determination of compressional wave velocity, the DSI excites a flexural mode in the borehole that can be used to determine shear-wave velocity in all types of formations. When the formation shear-wave velocity is less than the borehole fluid

F12. Diagram of the dipole shear sonic imager, p. 44.

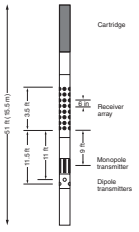

velocity, particularly in unconsolidated sediments, the flexural wave travels at shear-wave velocity and is the most reliable means to estimate that velocity. The configuration of the DSI also allows recording of crossline dipole waveforms. These modes can be used to estimate shear-wave splitting caused by preferred mineral and/or structural orientations in consolidated formations. A low-frequency source enables Stoneley waveforms to be acquired as well.

General Purpose Inclinometry Tool

The general purpose inclinometry tool (GPIT) uses acceleration measurements to calculate the amount of tool displacement that occurs during logging. The GPIT contains a triple-axis accelerometer and a triple-axis magnetometer. The GPIT records the orientation of the FMS images and allows more precise determination of log depths than can be determined from cable length, which may experience stretching and/or be affected by ship heave.

Formation MicroScanner

The FMS produces high-resolution microresistivity images. This tool consists of four orthogonal imaging pads, each containing 16 microelectrodes (Fig. **F13**). The pads, which are in direct contact with the borehole wall, emit a focused current into the formation. The current intensity fluctuations are measured and then converted to color images that reflect microresistivity variations: the lighter the color, the greater the resistivity (Ekstrom et al., 1987). These images have a vertical resolution of ~0.5 cm and a measurement interval of 0.25 cm (Serra, 1989). Roughly 30% of a 25-cm-diameter borehole is imaged. The advantage of the FMS is that the formation can be viewed in its complete state and often can be grouped into facies assemblages. Features such as bedding, fracturing, slump folding, and bioturbation can be resolved, and the fact that the images are oriented means that fabric can be analyzed and bed orientations can be measured.

F13. Diagram of the Formation MicroScanner, p. 45.

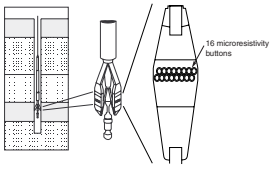

IN SITU TEMPERATURE AND PRESSURE MEASUREMENTS

In situ sediment thermal measurements were made during Leg 190 using the Adara APC temperature tool, the WSTP, and the Davis-Villinger temperature probe (DVTP) (Davis et al., 1997). Formation pore pressures were also measured using a prototype DVTP modified to include a pressure port and sensor. The instruments and procedures are summarized below.

Adara APC Temperature Tool

The Adara temperature tool fits directly into the cutting shoe on the APC and can therefore be used to measure sediment temperatures during regular piston coring. The tool consists of electronic components, including battery packs and a data logger, and a platinum resistance-temperature device calibrated over a temperature range of 0°–30°C. A photograph of the components can be found in Fisher and Becker (1993). The thermal time constant of the cutting shoe assembly into

which the Adara tool is inserted is ~2–3 min. The only modification to normal APC procedures required to obtain temperature measurements is to hold the corer in place for ~10 min after cutting the core. During this time, the Adara tool equilibrates toward the in situ temperature of the sediments.

The Adara tool logs data on a microprocessor contained within the instrument. Following deployment, the data are downloaded for processing on PC computers. The tool can be preprogrammed to record temperatures at a range of sampling rates. Sampling rates of 5 s were used during Leg 190.

A typical APC measurement consists of a mudline temperature record lasting 10 min for the first deployment at each borehole and 2 min on subsequent runs, a pulse of frictional heating when the piston is fired, a period of thermal decay that is monitored for 10 min, and a frictional pulse upon removal of the corer. Before reduction and drift corrections, nominal accuracy of Adara temperature data is estimated at 0.1°C.

WSTP Temperature Measurements

The WSTP can be configured with or without a fluid-sampling capability. When the probe tip is configured for temperature measurement only, the tip has a shorter time constant such that (1) the frictional heat pulse associated with insertion of the probe can be assumed to approximate more closely a line source of heat and (2) insertion of the instrument is less likely to fracture semilithified sediments.

In operation, the WSTP is mounted inside a core barrel and lowered down the drill pipe by wireline while the bit is held above the bottom of the hole. The tool is held briefly above the mudline to measure the temperature of bottom water. The tool is then lowered and latched into place, with the probe tip extending 1.1 m ahead of the bit. The drill string is lowered, and the probe is forced into the bottom of the hole. A colleted delivery system allows the probe to retract inside the bit if the formation is too hard to penetrate. With an APC/XCB bottom hole assembly, the bit can be decoupled from the tool after penetration so that the probe will not be disturbed by drill-string heave. Insertion of the probe significantly disturbs formation temperatures. If the instrument can not be left in position to allow this disturbance to decay completely, extrapolation to thermal equilibrium is required.

Davis-Villinger Temperature Probe

The DVTP is described in detail by Davis et al. (1997). The probe is conical and has two thermistors, one 1 cm from the tip of the probe and the other 12 cm above the tip. A third thermistor, referred to as the internal thermistor, is in the electronics package. Thermistor sensitivity is 1 mK in an operating range of –5° to 20°C, and the total operating range is –5° to 100°C. The thermistors were calibrated at the factory and on the laboratory bench before installation in the probe. In addition to the thermistors, the probe contains an accelerometer sensitive to 0.98 m/s^2. Both peak and mean acceleration are recorded by the logger. The accelerometer data are used to track disturbances to the instrument package during the equilibration interval.

In a DVTP deployment, mudline temperatures (within the drill pipe) are measured for 10 min during the first run within each hole and for 2 min during subsequent runs, before descent into the hole for a 10-min equilibration interval in the bottom. The time constants for the sensors

are ~1 min for the probe tip thermistor and ~2 min for the thermistor at 12 cm from the tip. Only data from the probe tip thermistor were used for estimation of in situ temperatures.

Thermal Data Reduction

Similar data reduction procedures were used for the three temperature tools. The transient thermal decay curves for sediment thermal probes are known to be a function of the geometry of the probes and the thermal properties of the probe and the sediments (Bullard, 1954; Horai and Von Herzen, 1985). Analysis of data requires fitting the measurements to analytical or synthetic decay curves calculated based on tool geometry, sampling interval, and tool and sediment thermal properties. For the DVTP tool, thermal decay data are analyzed by comparison to computed type curves using the software program CONEFIT, developed by Davis et al. (1997). However, it is generally not possible to obtain a perfect match between the synthetic curves and the data because (1) the probe does not reach thermal equilibrium during the penetration period; (2) contrary to ideal theory, the frictional pulse upon insertion is not instantaneous; and (3) temperature data are sampled at discrete intervals, so that the exact time of penetration is uncertain. Thus, both the effective penetration time and equilibrium temperature must be estimated by applying a fitting procedure, which involves shifting the synthetic curves in time to obtain a match with the recorded data. The data collected more than 20–50 s beyond penetration usually provide a reliable estimate of equilibrium temperature. The thermal decay curves for the measurements were initially fit on board assuming formation thermal conductivity of 1.0 W/(m·°C) for all of the data. Thermal conductivities measured in the shipboard laboratories (see **"Physical Properties,"** p. 19) were used for final estimation of in situ temperatures and for calculation of heat flow. Laboratory thermal conductivity measurements were not corrected for in situ conditions.

Davis-Villinger Temperature/Pressure Probe

Prior to Leg 190, one of the DVTP tools was modified at the Geological Survey of Canada as a prototype to allow simultaneous measurement of formation temperature and pressure. A new tip was designed that incorporates both a single thermistor in an oil-filled needle and ports to allow hydraulic transmission of fluid pressures outside the probe to a precision Paroscientific pressure gauge within the probe. A standard data logger was modified to accept the pressure signal instead of the second thermistor signal in the normal DVTP described above.

In 1999, the prototype was successfully tested on a wire from an oceanographic ship in sediments in 2600 m of water on the eastern flank of the Juan de Fuca Ridge (E. Davis, R. Macdonald, and R. Meldrum, unpubl. data). These tests demonstrated that (1) the thermal response of the modified tip remains virtually identical to that of the unmodified DVTP and (2) smooth pressure decay curves are recorded after penetration, such that useful extrapolations to in situ pore pressures are possible with measurement times on the order of 30 min. This pressure response is qualitatively similar to but slower than the thermal response, and the model for the characteristic response of pressure to the displacement and sediment deformation associated with penetration is more complex than the model used to estimate in situ temperatures from the decay of the frictional heating pulse. Construction of a com-

plete analytical or numerical model of the pressure response had not been completed by the time of Leg 190, so the stations were recorded for 30 min or as long as deemed operationally safe, and shipboard extrapolations to estimated formation pressures must be considered preliminary until thoroughly processed postcruise.

SEISMIC STRATIGRAPHY

The lithostratigraphic units at each of the Leg 190 drill sites were correlated with two-dimensional seismic reflection data collected in 1987 (Moore et al., 1990, 1991) and a three-dimensional seismic reflection data set collected in 1997 (Bangs et al., 1999; Moore et al., 1999). The 1987 lines were stacked and depth migrated using velocities models from two-ship wide-angle refraction data also collected in 1987 (Stoffa et al., 1992). Initial depth sections of the 3-D lines were made during Leg 190 based on these depth models. Refined depth conversions were made using the total depths of the drilled holes. Physical properties and logging data were used to help correlate the site lithostratigraphy with the seismic data. Because the depth sections are not well constrained, the depth correlations with lithostratigraphic units should be considered preliminary and subject to change when better depth sections are constructed.

REFERENCES

ASTM, 1989. Standard test method for laboratory miniature vane shear test for saturated fine-grained clayey soil. *Annual Book of ASTM Standards* (Vol. 04.08): Philadelphia (Am. Soc. Testing and Mater.), D4648-87:868–873.

Bangs, N.L., Taira, A., Kuramoto, S., Shipley, T.H., Moore, G.F., Mochizuki, K., Gulick, S.S., Zhao, Z., Nakamura, Y., Park, J.-O., Taylor, B.L., Morita, S., Ito, S., Hills, D.J., Leslie, S.C., Alex, C.M., McCutcheon, A.J., Ike, T., Yagi, H., and Toyama, G., 1999. U.S.-Japan collaborative 3-D seismic investigation of the Nankai Trough plate-boundary interface and shallowmost seismogenic zone. *Eos,* 80:F569.

Barnes, R.O., 1988. ODP in-situ fluid sampling and measurement: a new wireline tool. *In* Mascle, A., Moore, J.C., et al., *Proc. ODP, Init. Repts.,* 110: College Station, TX (Ocean Drilling Program), 55–63.

Blum, P., 1997. Physical properties handbook: a guide to the shipboard measurement of physical properties of deep-sea cores. *ODP Tech. Note,* 26 [Online]. Available from World Wide Web: <http://www-odp.tamu.edu/publications/tnotes/tn26/INDEX.HTM>.

Boyce, R.E., 1976. Definitions and laboratory techniques of compressional sound velocity parameters and wet-water content, wet-bulk density, and porosity parameters by gravimetric and gamma-ray attenuation techniques. *In* Schlanger, S.O., Jackson, E.D., et al., *Init. Repts. DSDP,* 33: Washington (U.S. Govt. Printing Office), 931–958.

Bullard, E.C., 1954. The flow of heat through the floor of the Atlantic Ocean. *Proc. R. Soc. London A,* 222:408–429.

Cande, S.C., and Kent, D.V., 1995. Revised calibration of the geomagnetic polarity timescale for the Late Cretaceous and Cenozoic. *J. Geophys. Res.,* 100:6093–6095.

Claypool, G.E., and Kvenvolden, K.A., 1983. Methane and other hydrocarbon gases in marine sediment. *Annu. Rev. Earth Planet. Sci.,* 11:299–327.

Davis, E.E., Villinger, H., MacDonald, R.D., Meldrum, R.D., and Grigel, J., 1997. A robust rapid-response probe for measuring bottom-hole temperatures in deep-ocean boreholes. *Mar. Geophys. Res.,* 19:267–281.

Ekstrom, M.P., Dahan, C., Chen, M.-Y., Lloyd, P., and Rossi, D.J., 1987. Formation imaging with microelectrical scanning arrays. *Log Analyst,* 28:294–306.

Ellis, D.V., 1987. *Well Logging for Earth Scientists:* New York (Elsevier).

Fisher, A.T., and Becker, K., 1993. A guide to ODP tools for downhole measurements. *ODP Tech. Note,* 10.

Fisher, A.T., and Underwood, M.B., 1995. Calibration of an X-ray diffraction method to determine relative mineral abundances in bulk powders using matrix singular value decomposition: a test from the Barbados accretionary complex. *In* Shipley, T.H., Ogawa, Y., Blum, P., et al., *Proc. ODP, Init. Repts.,* 156: College Station, TX (Ocean Drilling Program), 29–37.

Fry, J.C., 1988. Determination of biomass. *In* Austin, B. (Ed.), *Methods in Aquatic Bacteriology:* Chichester (Wiley), 27–72.

Gartner, S., 1977. Calcareous nannofossil biostratigraphy and revised zonation of the Pleistocene. *Mar. Micropaleontol.,* 2:1–25.

Gieskes, J.M., Gamo, T., and Brumsack, H., 1991. Chemical methods for interstitial water analysis aboard *JOIDES Resolution. ODP Tech. Note,* 15.

Goldberg, D., 1990. Test performance of the Ocean Drilling Program wireline heave motion compensator. *Sci. Drill.,* 1:206–209.

Harvey, P.K., Lovell, M.A., Brewer, T.S., Locke, J., and Mansley, E., 1996. Measurement of thermal neutron absorption cross section in selected geothermal reference materials. *Geostand. Newsl.,* 20:79–85.

Hoppie, B.W., Blum, P., and the Shipboard Scientific Party, 1994. Natural gamma-ray measurements on ODP cores: introduction to procedures with examples from Leg

150. *In* Mountain, G.S., Miller, K.G., Blum, P., et al., *Proc. ODP, Init. Repts.,* 150: College Station, TX (Ocean Drilling Program), 51–59.

Horai, K., and Von Herzen, R.P., 1985. Measurement of heat flow on Leg 86 of the Deep Sea Drilling Project. *In* Heath, G.R., Burckle, L.H., et al., *Init. Repts. DSDP,* 86: Washington (U.S. Govt. Printing Office), 759–777.

Kimura, G., Silver, E.A., Blum, P., et al., 1997. *Proc. ODP, Init. Repts.,* 170: College Station, TX (Ocean Drilling Program).

Kvenvolden, K.A., 1985. Comparison of marine gas hydrates in sediments of an active and passive margin. *Mar. Pet. Geol.,* 2:65–71.

Lovell, M.A., Harvey, P.K., Brewer, T.S., Williams, C., Jackson, P.D., and Williamson, G., 1998. Application of FMS images in the Ocean Drilling Program: an overview. *In* Cramp, A., MacLeod, C.J., Lee, S.V., and Jones, E.J.W. (Eds.), *Geological Evolution of Ocean Basins: Results from the Ocean Drilling Program.* Geol. Soc. Spec. Publ. London, 131:287–303.

Lowrie, W., 1990. Identification of ferromagnetic minerals in a rock by coercivity and unblocking temperature properties. *Geophys. Res. Lett.,* 17:159–162.

Lundberg, N., and Moore, J.C., 1986. Macroscopic structural features in Deep Sea Drilling Project cores from forearc regions. *In* Moore, J.C. (Ed.), *Structural Fabric in Deep Sea Drilling Project Cores From Forearcs.* Mem.—Geol. Soc. Am., 166:13–44.

Manheim, F.T., and Sayles, F.L., 1974. Composition and origin of interstitial waters of marine sediments, based on deep sea drill cores. *In* Goldberg, E.D. (Ed.), *The Sea* (Vol. 5): *Marine Chemistry: The Sedimentary Cycle:* New York (Wiley), 527–568.

Martini, E., 1971. Standard Tertiary and Quaternary calcareous nannoplankton zonation. *In* Farinacci, A. (Ed.), *Proc. 2nd Int. Conf. Planktonic Microfossils Roma:* Rome (Ed. Tecnosci.), 2:739–785.

Mazzullo, J., and Graham, A.G. (Eds.), 1988. *Handbook for Shipboard Sedimentologists.* ODP Tech. Note, 8.

Mazzullo, J.M., Meyer, A., and Kidd, R.B., 1988. New sediment classification scheme for the Ocean Drilling Program. *In* Mazzullo, J., and Graham, A.G. (Eds.), *Handbook for Shipboard Sedimentologists.* ODP Tech. Note, 8:45–67.

Moore, G.F., Karig, D.E., Shipley, T.H., Taira, A., Stoffa, P.L., and Wood, W.T., 1991. Structural framework of the ODP Leg 131 area, Nankai Trough. *In* Taira, A., Hill, I., Firth, J.V., et al., *Proc. ODP, Init. Repts.,* 131: College Station, TX (Ocean Drilling Program), 15–20.

Moore, G.F., Shipley, T.H., Stoffa, P.L., Karig, D.E., Taira, A., Kuramoto, S., Tokuyama, H., and Suyehiro, K., 1990. Structure of the Nankai Trough accretionary zone from multichannel seismic reflection data. *J. Geophys. Res.,* 95:8753–8765.

Moore, G.F., Taira, A., Kuramoto, S., Shipley, T.H., and Bangs, N.L., 1999. Structural setting of the 1999 U.S.-Japan Nankai Trough 3-D seismic reflection survey. *Eos,* 80:F569.

Parkes, R.J., Cragg, B.A., Bale, S.J., Getliff, J.M., Goodman, K., Rochelle, P.A., Fry, J.C., Weightman, A.J., and Harvey, S.M., 1994. A deep bacterial biosphere in Pacific Ocean sediments. *Nature,* 371:410–413.

Paull, C.K., Matsumoto, R., Wallace, P.J., et al., 1996. *Proc. ODP, Init. Repts.,* 164: College Station, TX (Ocean Drilling Program).

Rider, M., 1990. Gamma-ray log shape used as a facies indicator: critical analysis of an oversimplified method. *In* Hurst, A., Lovell, M.A., and Morton, A.C. (Eds.), *Geological Application of Wireline Logs.* Geol. Soc. Spec. Publ. London, 48:27–37.

————, 1996. *The Geological Interpretation of Well Logs* (2nd ed.): Caithness (Whittles Publishing).

Schlumberger, 1989. *Log Interpretation Principles/Applications:* Houston (Schlumberger Educ. Services), SMP–7017.

————, 1994. *IPL Integrated Porosity Lithology:* Houston (Schlumberger Wireline and Testing), SMP-9270.

————, 1995. *DSI—Dipole Sonic Imager:* Houston (Schlumberger Wireline and Testing), SMP-5128.

Schneider, R.R., Cramp, A., Damuth, J.E., Hiscott, R.N., Kowsmann, R.O., Lopez, M., Nanayama, F., Normark, W.R., and Shipboard Scientific Party, 1995. Color-reflectance measurements obtained from Leg 155 cores. *In* Flood, R.D., Piper, D.J.W., Klaus, A., et al., *Proc. ODP, Init. Repts.,* 155: College Station, TX (Ocean Drilling Program), 697–700.

Serra, O., 1984. *Fundamentals of Well-Log Interpretation* (Vol. 1): *The Acquisition of Logging Data:* Dev. Pet. Sci., 15A: Amsterdam (Elsevier).

————, 1986. *Fundamentals of Well-Log Interpretation* (Vol. 2): *The Interpretation of Logging Data*. Dev. Pet. Sci., 15B.

————, 1989. *Formation MicroScanner Image Interpretation:* Houston (Schlumberger Educ. Services), SMP-7028.

Serra, O., and Sulpice, L., 1975. Sedimentological analysis of shale-sand series from well logs. *Trans. SPWLA 16th Ann. Logging Symp.,* Pap. W.

Shipboard Scientific Party, 1991. Explanatory notes. *In* Taira, A., Hill, I., Firth, J.V., et al., *Proc. ODP, Init. Repts.,* 131: College Station, TX (Ocean Drilling Program), 25–60.

————, 1995. Explanatory notes. *In* Shipley, T.H., Ogawa, Y., Blum, P., et al., *Proc. ODP, Init. Repts.,* 156: College Station, TX (Ocean Drilling Program), 39–68.

————, 1997. Explanatory notes. *In* Kimura, G., Silver, E., Blum, P., et al., *Proc. ODP, Init. Repts.,* 170: College Station, TX (Ocean Drilling Program), 19–42.

Shipley, T.H., Ogawa, Y., Blum, P., et al., 1995. *Proc. ODP, Init. Repts.,* 156: College Station, TX (Ocean Drilling Program).

Smith, D.C., Spivack, A.J., Fisk, M.R., Haveman, S.A., Staudigel, H., and ODP Leg 185 Scientific Party, 2000. Methods for quantifying potential microbial contamination during deep ocean coring. *ODP Tech. Note,* 28 [Online]. Available from World Wide Web: <http://www-odp.tamu.edu/publications/tnotes/tn28/INDEX.HTM>.

Stoffa, P.L., Wood, W.T., Shipley, T.H., Moore, G.F., Nishiyama, E., Bothelo, M.A.B., Taira, A., Tokuyama, H., and Suyehiro, K., 1992. Deepwater high-resolution expanding spread and split spread marine seismic profiles in the Nankai Trough. *J. Geophys. Res.,* 97:1687–1713.

Taira, A., Hill, I., Firth, J.V., et al., 1991. *Proc. ODP, Init. Repts.,* 131: College Station, TX (Ocean Drilling Program).

Timur, A., and Toksöz, M.N., 1985. Downhole geophysical logging. *Annu. Rev. Earth Planet. Sci.,* 13:315–344.

Tittman, J., 1986. *Geophysical Well Logging:* London (Academic Press).

Von Herzen, R.P., and Maxwell, A.E., 1959. The measurement of thermal conductivity of deep-sea sediments by a needle-probe method. *J. Geophys. Res.,* 64:1557–1563.

Wellsbury, P., Goodman, K., Barth, T., Cragg, B.A., Barnes, S.P., and Parkes, R.J., 1997. Deep marine biosphere fueled by increasing organic matter availability during burial and heating. *Nature,* 388:573–576.

Widdel, F., and Bak, F., 1992. Gram negative mesophilic sulfate reducing bacteria. *In* Ballows, A., et al. (Eds.): *The Prokaryotes* (Vol. 4): New York (Springer-Verlag), 3352–3378.

Young, J.R., 1998. Neogene. *In* Bown, P.R. (Ed.), *Calcareous Nannofossil Biostratigraphy* (Vol. 8): Dordrecht (Kluwer Academic), 225–265.

Figure F1. Diagram illustrating core, section, and sample numbering.

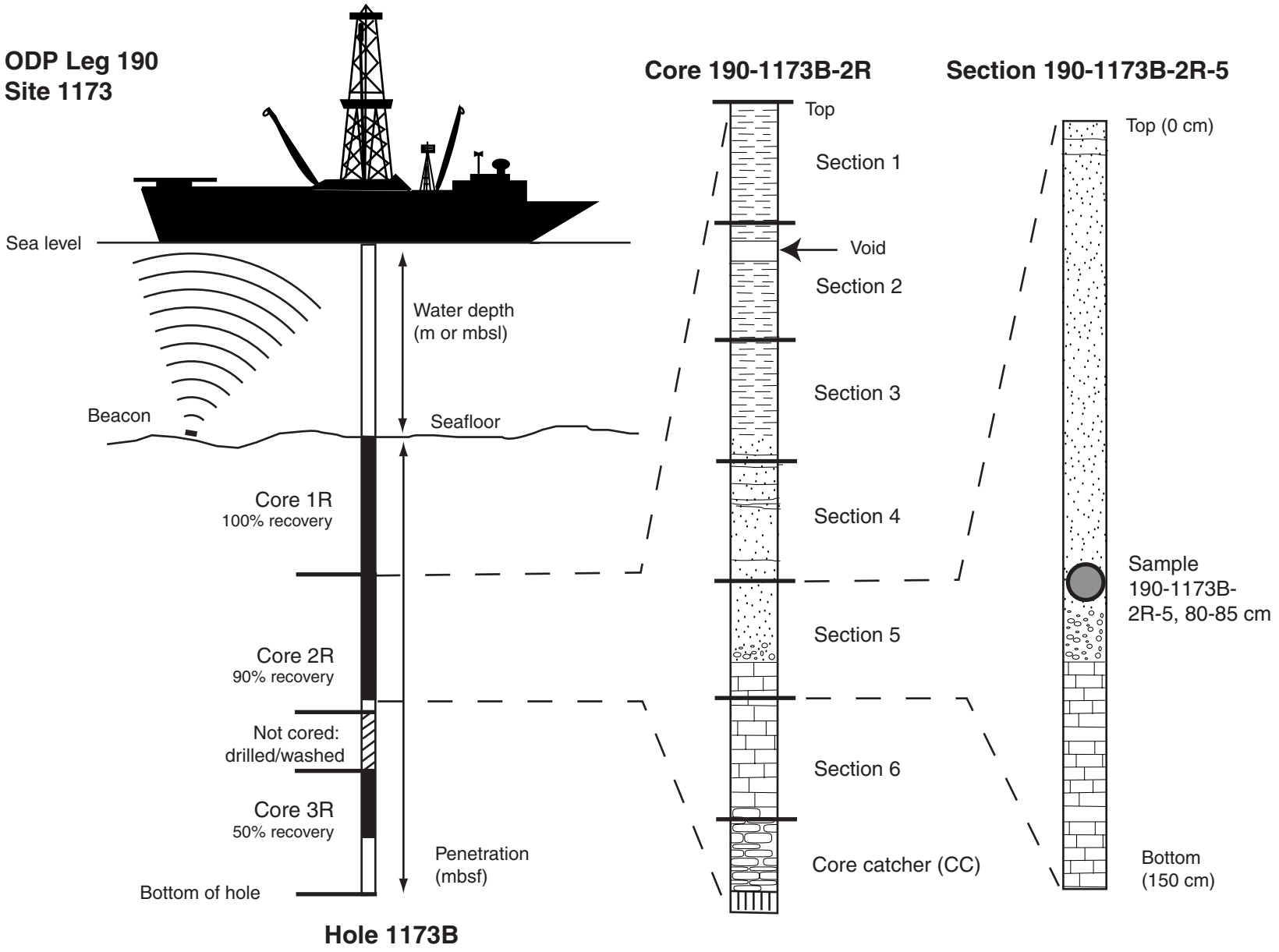

Figure F2. Graphic patterns used on AppleCORE barrel sheets to indicate lithologies encountered during Leg 190. Also shown are symbols for sedimentary structures, deformation features, samples, and coring/drilling disturbance in soft sediment and hard sedimentary rock.

Figure F3. Examples of X-ray diffractograms showing diagnostic peaks used to calculate peak areas for minerals in both standard mixtures and natural samples from the Nankai Trough.

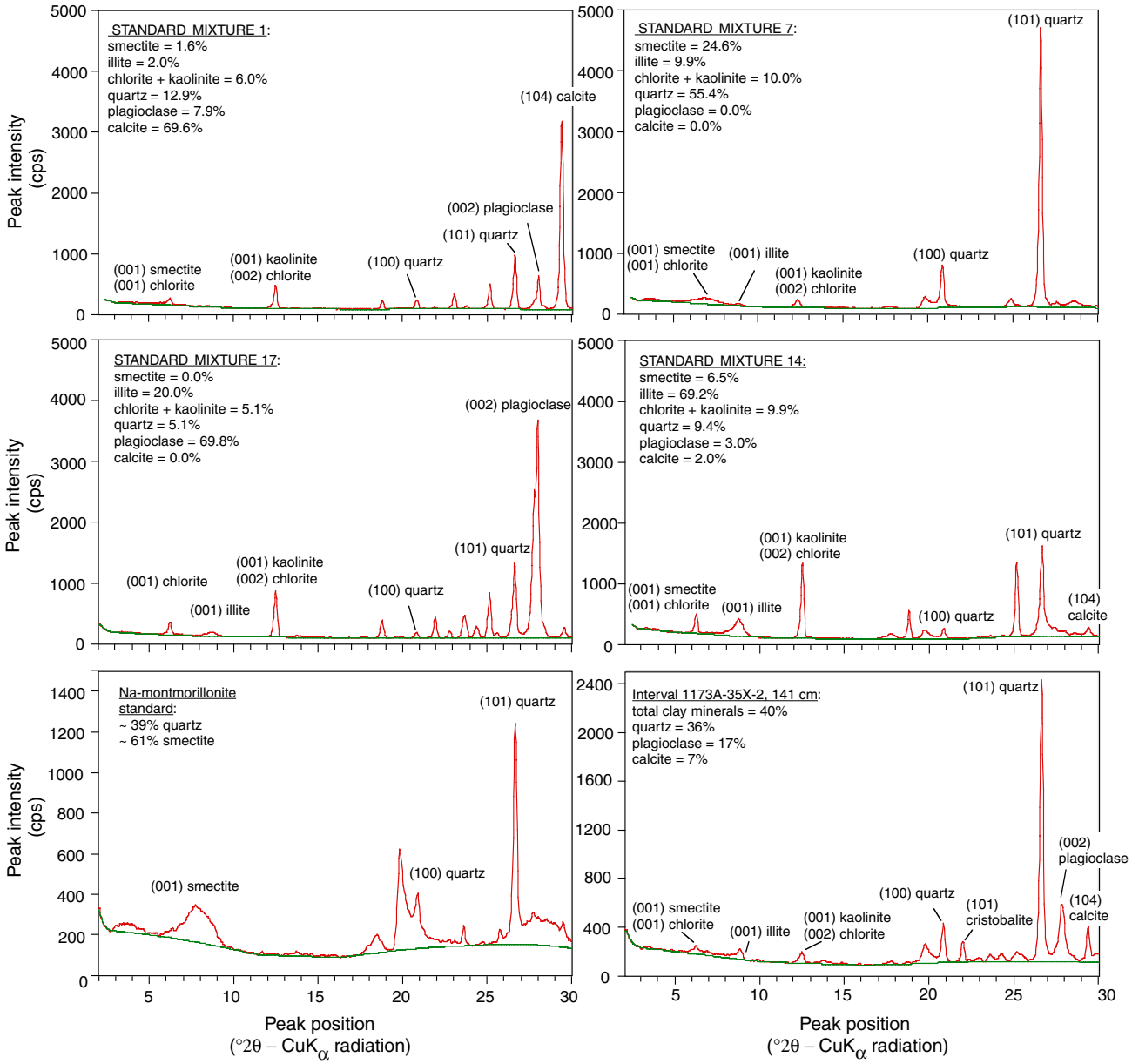

Figure F4. Layout of the structural description sheet.

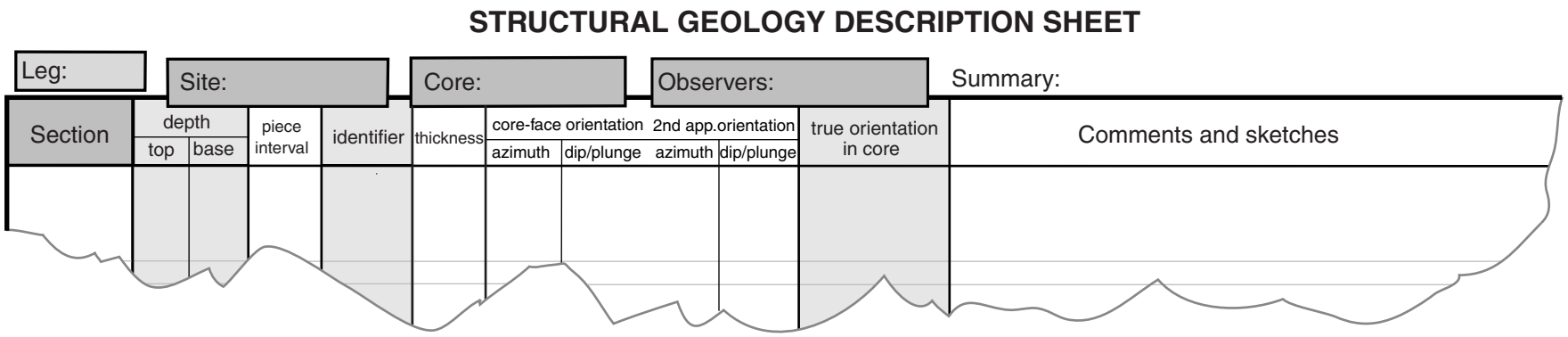

Figure F5. Protractor-goniometer used for measuring orientations of structures in the cores. (**A**) Drawing of device being used to (**B**) measure the dip of a structure on the face of a split core, (**C**) assess the dip of a structure as seen at right angles to the split-core face, and (**D**) measure the azimuth of a structure as seen on the upper surface of a core.

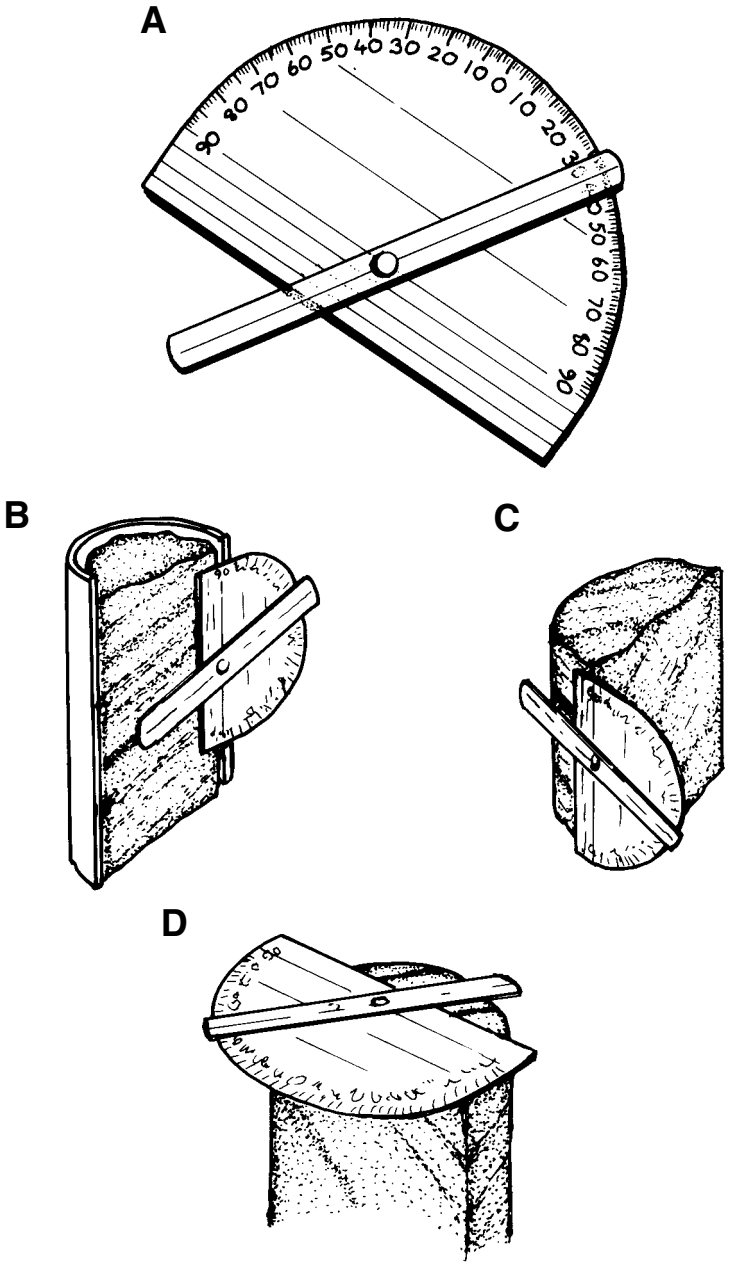

Figure F6. Diagram showing the conventions used during Leg 190 for measuring azimuths and dips of structural features in cores and the techniques adopted for measuring structural planes in three dimensions in the core reference frame. The core reference frame conventions for the (**A**) working and (**B**) archive half of the core. The E-W (core reference frame) apparent dip of a feature was measured first, generally on the face of the archive half. The data were recorded as an apparent dip toward either 090° or 270°. In this case the apparent dip is toward 270°. A second apparent dip is measured by making a cut parallel to the core axis but perpendicular to the core face in the working half of the core. Note that cuts were normally considerably smaller than the one represented in the diagram. The feature is identified on the new surface and the apparent dip in the north-south direction (core reference frame) marked with a toothpick. The (**C**) apparent dip is measured with a modified protractor and quoted as a value toward either 000° or 180°. In this case, the apparent dip is toward 000° (into the working half). True strike and dip of the surface in the core reference frame are calculated from the two apparent measurements.

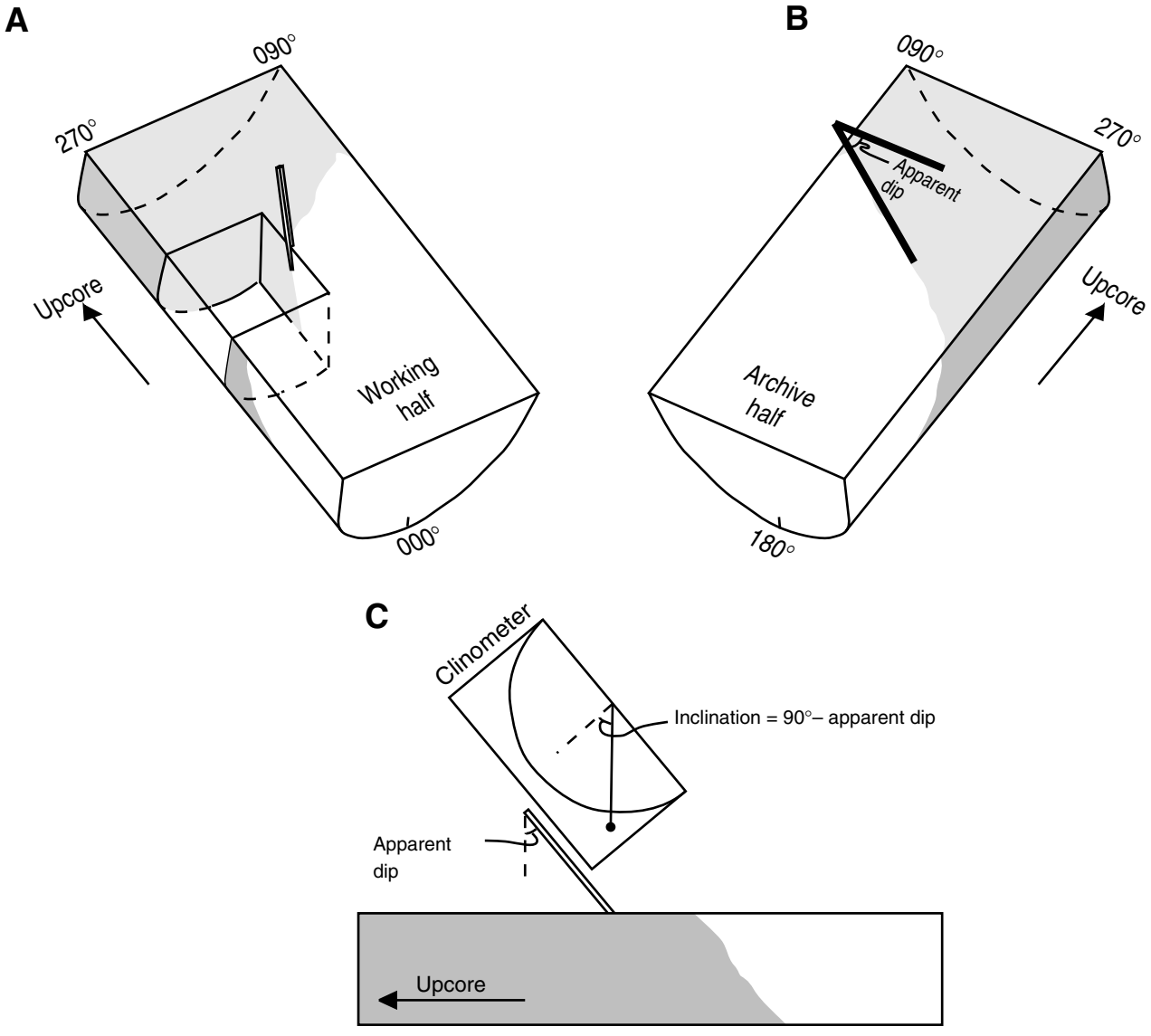

Figure F7. The gas permeameter used during Leg 190.

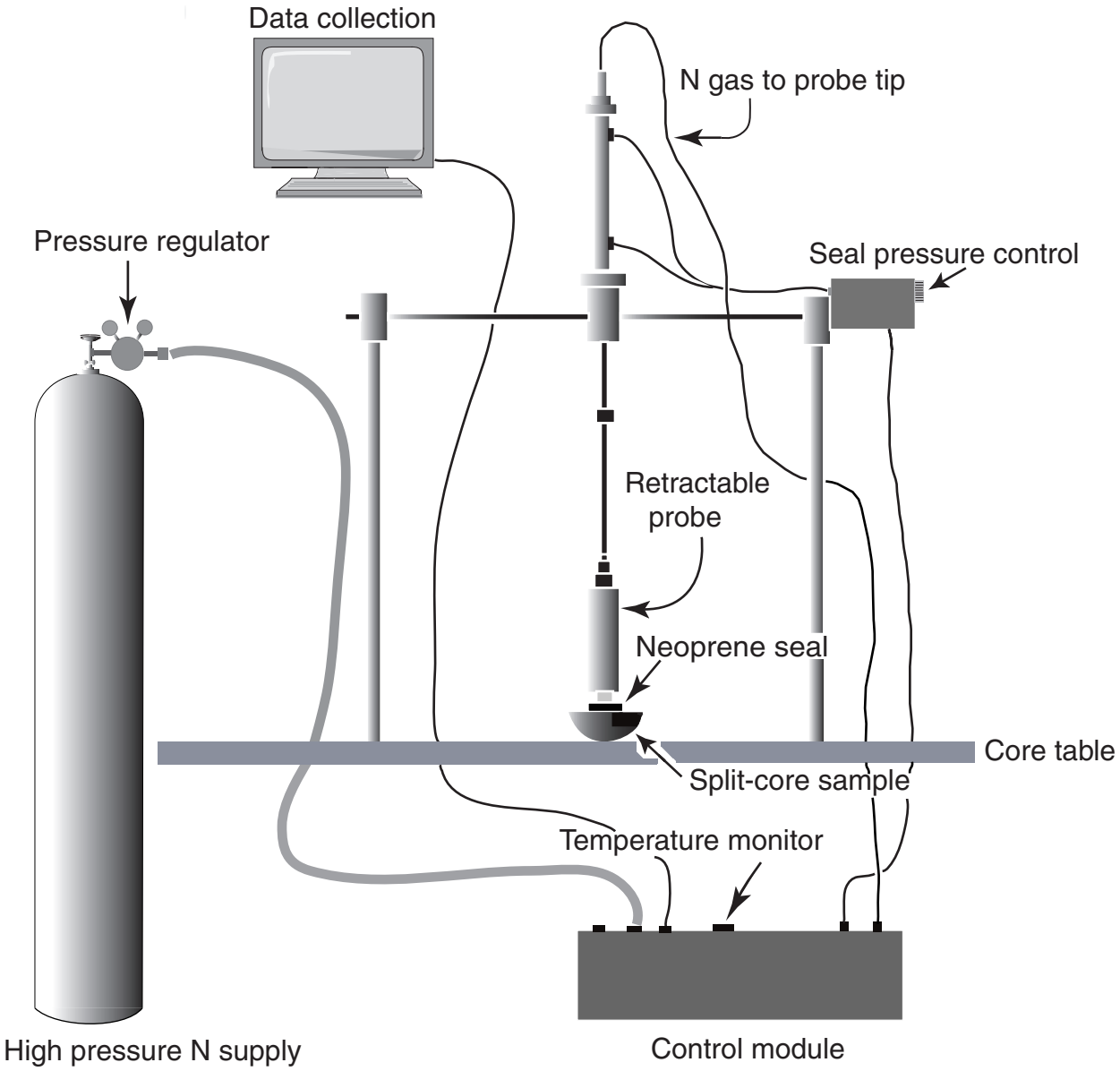

Figure F8. Biostratigraphic event zonal markers.

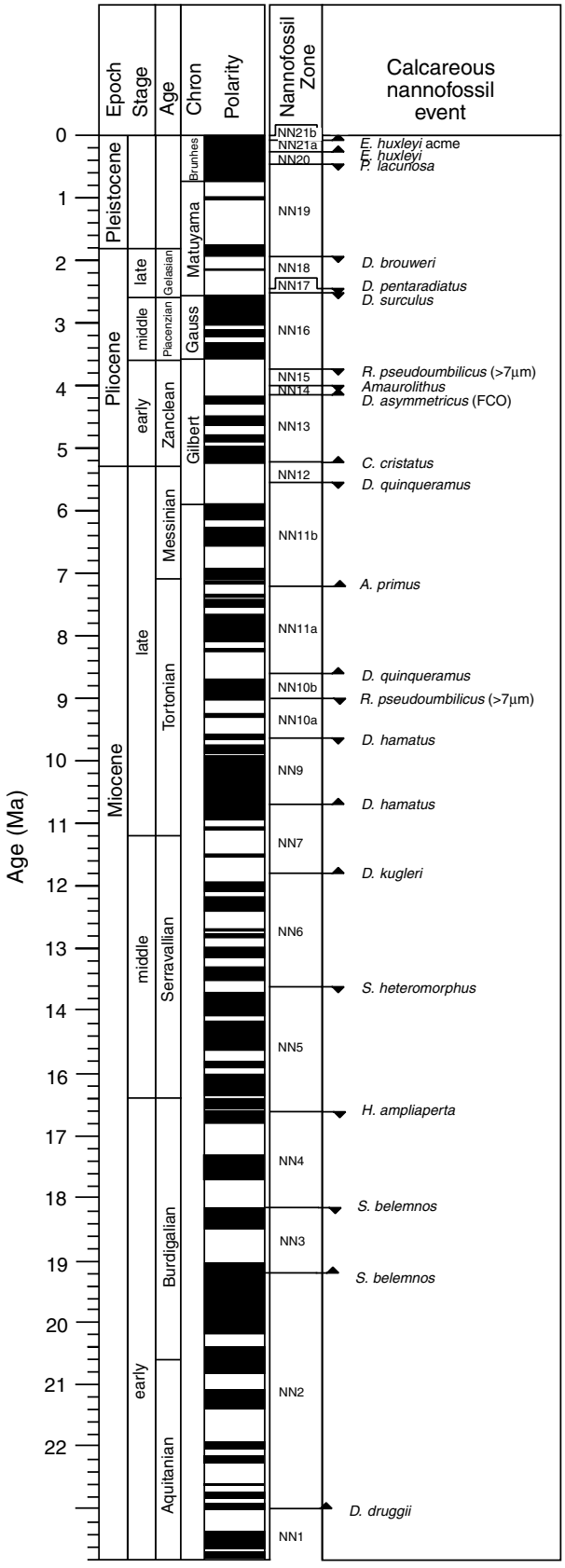

Figure F9. Paleomagnetic coordinate systems of ODP cores and discrete samples. **A.** Orientation of discrete samples. The z-axis of a plastic cube or minicore is in the opposite direction to that of a working-half core. **B.** The paleomagnetic measurement coordinate systems for both archive- and working-half cores.

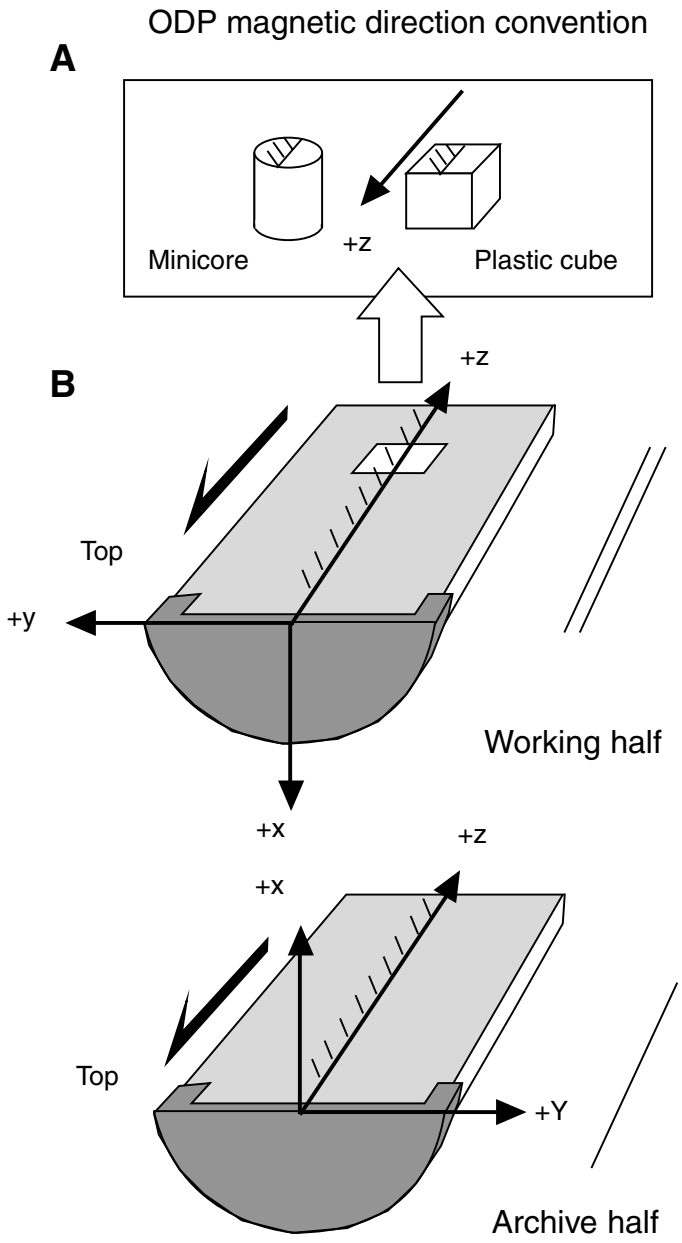

Figure F10. Magnetostratigraphic timetable used during Leg 190. The ages used are based on the Cande and Kent (1995) time scale.

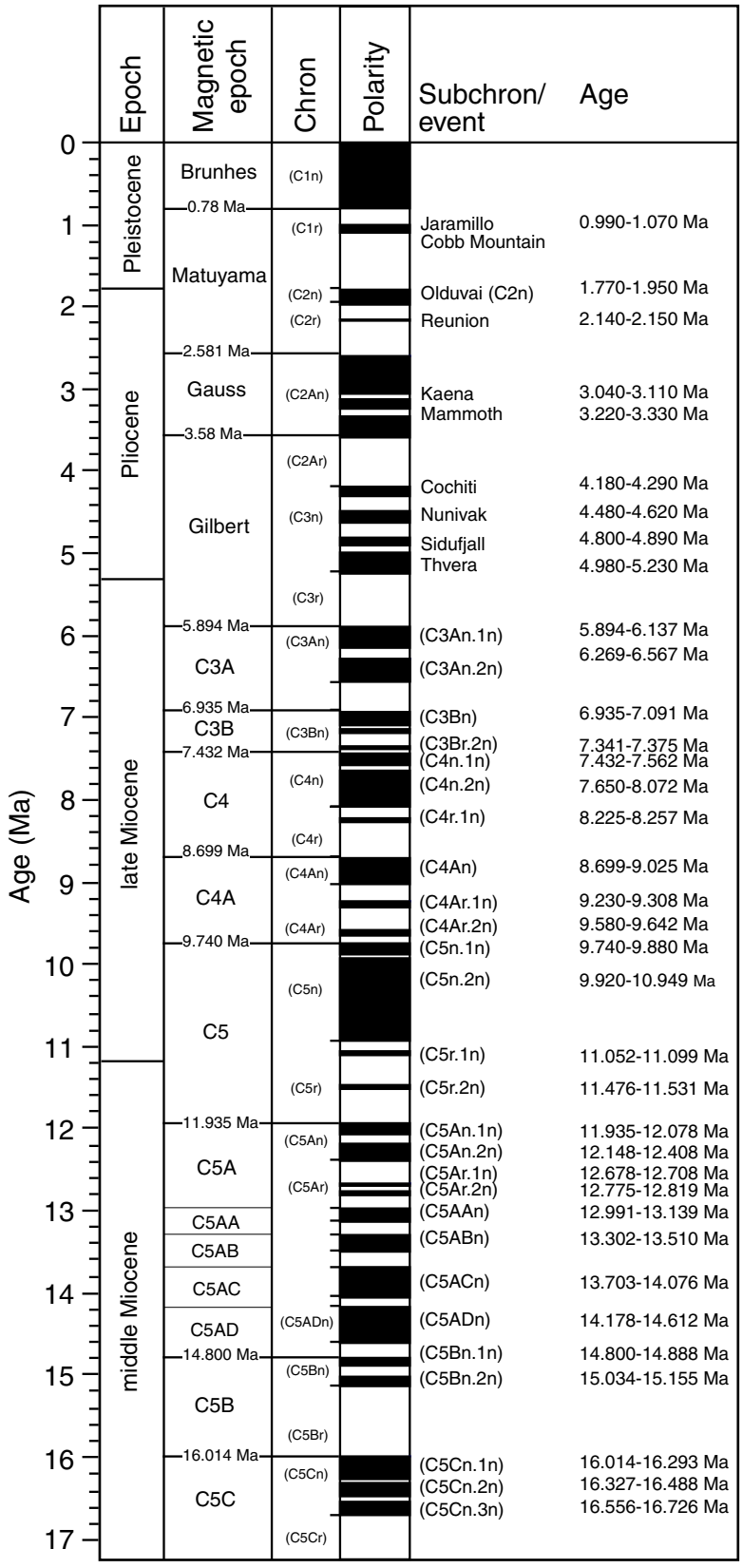

Figure F11. Wireline tool strings used during Leg 190.

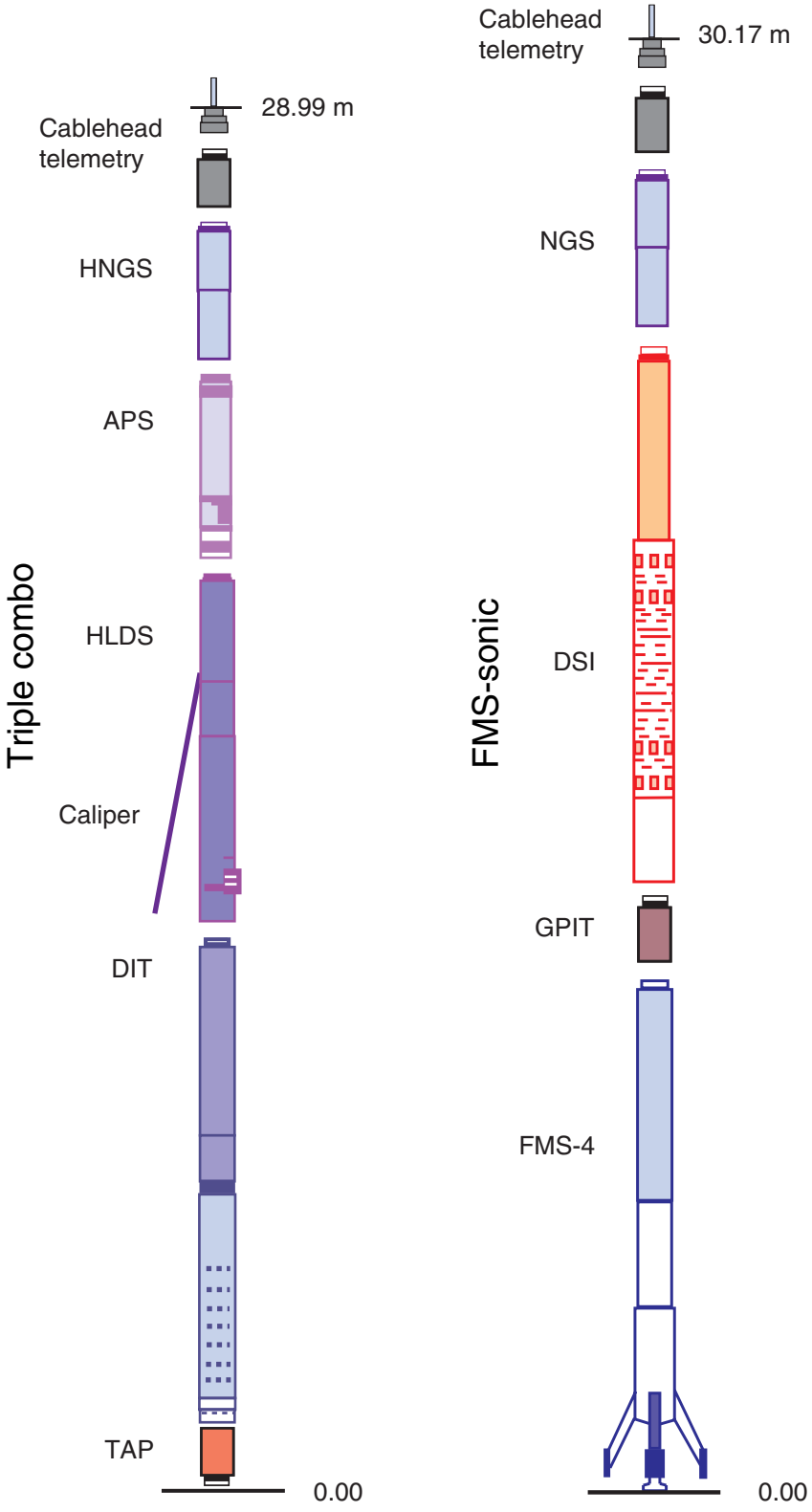

Figure F12. Diagram of the dipole shear sonic imager.

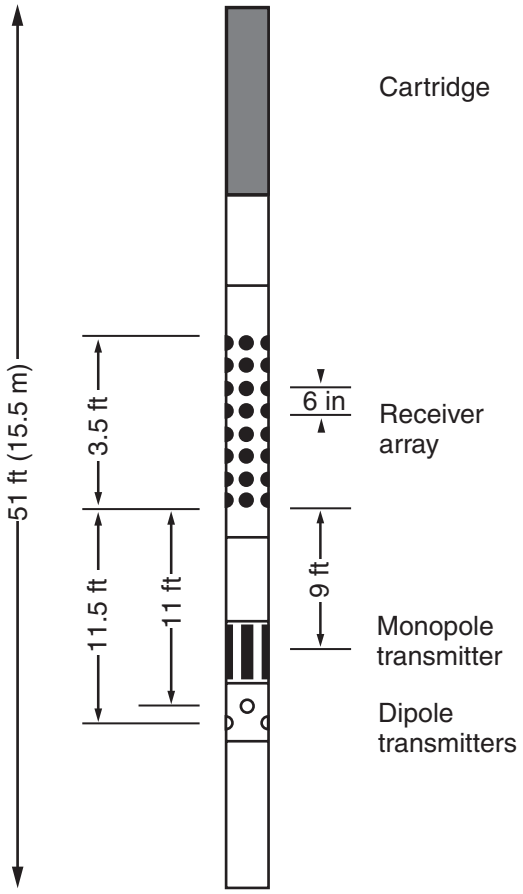

Figure F13. Diagram of the Formation MicroScanner (adapted from Lovell et al., 1998).

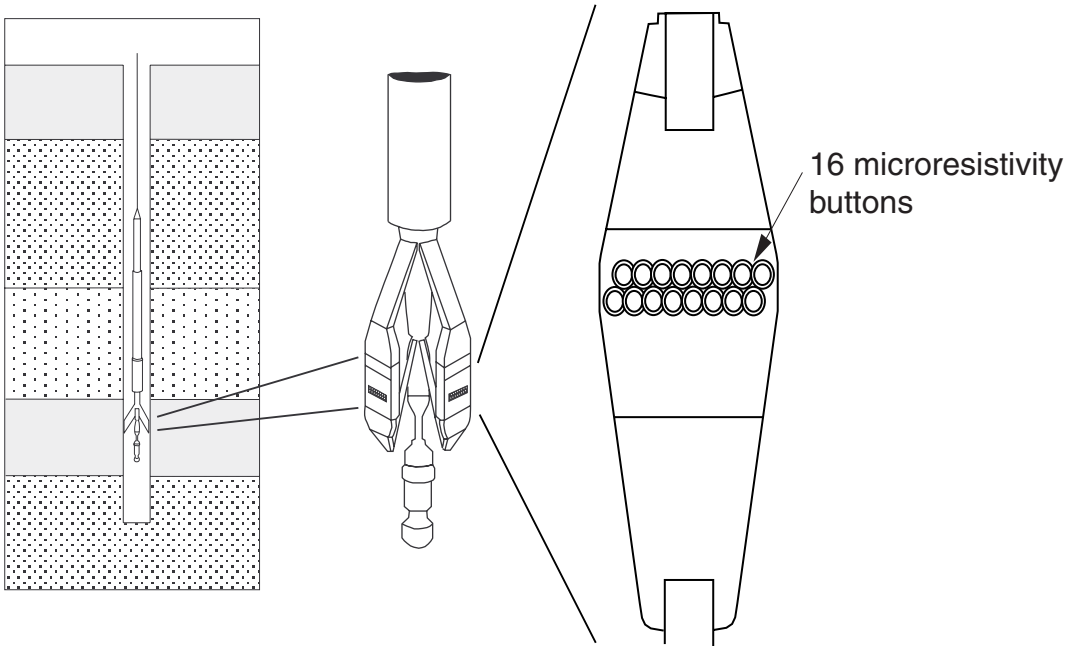

Table T1. Normalization factors for bulk-powder samples analyzed, Leg 190.

Indicator mineral	Target mineral					
	Smectite	Illite	Chlorite + kaolinite	Quartz	Plagioclase	Calcite
Smectite	$0.46154582 \times 10^{-2}$	$-0.40810031 \times 10^{-4}$	$-0.68136855 \times 10^{-4}$	$0.20990595 \times 10^{-2}$	$-0.24493772 \times 10^{-3}$	$-0.26646213 \times 10^{-3}$
Illite	$0.57179161 \times 10^{-3}$	$0.64763213 \times 10^{-2}$	$-0.22265653 \times 10^{-3}$	$-0.99226029 \times 10^{-3}$	$-0.36059471 \times 10^{-4}$	$-0.30476565 \times 10^{-3}$
Chlorite + kaolinite	$-0.12564977 \times 10^{-2}$	$0.37190966 \times 10^{-4}$	$0.80104225 \times 10^{-3}$	$-0.57112821 \times 10^{-3}$	$0.80048252 \times 10^{-4}$	$0.73785166 \times 10^{-4}$
Quartz	$-0.78230050 \times 10^{-5}$	$0.14331730 \times 10^{-4}$	$0.11500453 \times 10^{-3}$	$0.81108598 \times 10^{-3}$	$-0.11971233 \times 10^{-5}$	$-0.21123733 \times 10^{-4}$
Plagioclase	$-0.44256009 \times 10^{-4}$	$0.16375128 \times 10^{-4}$	$-0.42899275 \times 10^{-4}$	$-0.33711429 \times 10^{-4}$	$0.95490349 \times 10^{-3}$	$-0.36721394 \times 10^{-4}$
Calcite	$-0.10267436 \times 10^{-3}$	$0.57594101 \times 10^{-4}$	$0.14502202 \times 10^{-3}$	$0.54223674 \times 10^{-4}$	$0.42776024 \times 10^{-4}$	$0.17315382 \times 10^{-2}$

Notes: Calibration utilized 16 standard mineral mixtures. Factors are based on X-ray diffraction peak areas and determined with matrix singular value decomposition.

Table T2. Measured weight percentages of minerals in standard–mineral mixtures and their calculated abundances.

	Measured weight percentage							Weight percentage calculated from X-ray diffraction							Error (measured wt% – calculated wt%)						
Standard	Smectite	Illite	Chlorite + kaolinite	Total clay	Quartz	Plagioclase	Calcite	Smectite	Illite	Chlorite + kaolinite	Total clay	Quartz	Plagioclase	Calcite	Smectite	Illite	Chlorite + kaolinite	Clay	Quartz	Plagioclase	Calcite
SVD method:																					
1	4.3	0.0	10.1	14.4	14.9	5.3	65.4	1.6	2.0	6.0	9.6	12.9	7.9	69.6	2.7	–2.0	4.1	4.8	2.0	–2.6	–4.3
2	4.2	9.2	17.8	31.2	24.2	11.1	33.6	6.3	10.0	19.9	36.2	23.9	10.0	29.8	–2.1	–0.9	–2.1	–5.0	0.3	1.1	3.8
3	9.8	9.1	12.5	31.4	38.3	7.8	22.6	12.3	9.9	10.1	32.3	37.8	9.9	19.9	–2.5	–0.9	2.4	–0.9	0.5	–2.1	2.7
4	5.4	0.0	26.3	31.8	40.0	8.0	20.3	3.0	0.0	25.2	28.2	41.8	10.0	19.9	2.4	0.0	1.1	3.6	–1.8	–2.0	0.4
5	29.0	9.0	13.3	51.3	26.9	8.3	13.4	24.1	10.5	19.7	54.3	26.2	8.6	11.0	4.9	–1.5	–6.4	–3.0	0.7	–0.3	2.4
6	5.3	6.0	15.9	27.1	37.7	14.7	20.5	9.2	5.0	25.1	39.3	30.8	14.9	14.9	–3.9	1.0	–9.2	–12.2	6.9	–0.2	5.6
7	27.3	8.4	7.6	43.3	56.7	0.0	0.0	24.6	9.9	10.0	44.5	55.4	0.0	0.0	2.7	–1.6	–2.4	–1.2	1.3	0.0	0.0
8	0.0	19.7	13.0	32.7	38.3	15.5	13.6	4.9	20.0	21.9	46.8	31.1	12.0	10.0	–4.9	–0.3	–8.9	–14.1	7.2	3.5	3.6
9	8.4	19.1	14.3	41.8	34.6	13.8	9.8	6.1	19.6	11.8	37.5	38.1	14.7	9.8	2.3	–0.5	2.5	4.3	–3.5	–0.9	0.0
10	0.5	8.2	23.7	32.4	54.2	13.4	0.0	1.3	8.0	24.8	34.1	50.4	15.5	0.0	–0.8	0.2	–1.1	–1.7	3.8	–2.2	0.0
11	7.5	5.5	0.0	13.0	27.3	44.0	15.6	9.2	5.0	0.0	14.2	30.8	40.1	15.0	–1.7	0.5	0.0	–1.2	–3.5	3.9	0.6
12	2.5	14.7	11.0	28.2	33.2	33.5	5.2	3.0	14.9	10.0	27.9	36.9	29.9	5.2	–0.5	–0.2	1.0	0.3	–3.7	3.6	0.0
14	6.4	67.5	11.9	85.8	9.1	3.6	1.5	6.5	69.2	9.9	85.6	9.5	3.0	2.0	–0.1	–1.7	2.0	0.2	–0.4	0.6	–0.6
15	3.4	4.9	68.9	77.3	4.9	13.8	4.1	3.9	5.1	69.0	78.0	4.4	12.8	4.8	–0.5	–0.2	–0.1	–0.8	0.5	1.0	–0.8
16	9.0	3.3	11.1	23.4	64.1	5.6	6.9	8.2	2.0	3.0	13.2	74.0	4.9	7.9	0.8	1.3	8.1	10.2	–9.9	0.7	–1.0
17	2.6	20.5	5.5	28.6	7.6	63.9	0.0	0.0	20.0	5.1	25.1	5.1	69.8	0.0	2.6	0.5	0.4	3.5	2.5	–5.9	0.0
Linear regression method:																					
1	4.3	0.0	10.1	14.4	14.9	5.3	65.4	0.0	2.0	9.5	11.5	10.8	7.8	69.8	4.3	–2.0	0.6	2.9	4.1	–2.5	–4.5
2	4.2	9.2	17.8	31.2	24.2	11.1	33.6	12.6	8.2	16.4	37.2	21.2	10.7	30.9	–8.4	1.0	1.4	–6.0	3.0	0.4	2.7
3	9.8	9.1	12.5	31.4	38.3	7.8	22.6	11.2	9.5	12.0	32.7	33.1	10.4	23.8	–1.4	–0.4	0.5	–1.3	5.2	–2.6	–1.2
4	5.4	0.0	26.3	31.8	40.0	8.0	20.3	0.0	2.0	26.1	28.1	40.7	9.4	21.8	5.4	–2.0	0.2	3.7	–0.7	–1.4	–1.5
5	29.0	9.0	13.3	51.3	26.9	8.3	13.4	28.4	11.4	17.9	57.7	18.1	7.6	16.7	0.6	–2.4	–4.6	–6.4	8.8	0.7	–3.3
6	5.3	6.0	15.9	27.1	37.7	14.7	20.5	11.1	5.8	13.9	30.8	36.3	14.6	18.4	–5.8	0.2	2.0	–3.7	1.4	0.1	2.1
7	27.3	8.4	7.6	43.3	56.7	0.0	0.0	20.6	10.6	8.2	39.4	59.0	1.5	0.0	6.7	–2.3	–0.6	3.9	–2.3	–1.5	0.0
8	0.0	19.7	13.0	32.7	38.3	15.5	13.6	4.4	17.8	11.8	34.0	39.0	14.6	12.4	–4.4	1.9	1.2	–1.3	–0.7	0.9	1.2
9	8.4	19.1	14.3	41.8	34.6	13.8	9.8	11.8	17.9	13.6	43.3	32.7	13.9	10.0	–3.4	1.2	0.7	–1.5	1.9	–0.1	–0.2
10	0.5	8.2	23.7	32.4	54.2	13.4	0.0	0.0	8.2	21.4	29.6	56.3	14.2	0.0	0.5	0.0	2.3	2.8	–2.1	–0.9	0.0
11	7.5	5.5	0.0	13.0	27.3	44.0	15.6	5.3	5.1	5.3	15.7	27.1	38.6	18.6	2.2	0.4	–5.3	–2.7	0.2	5.4	–3.0
12	2.5	14.7	11.0	28.2	33.2	33.5	5.2	7.2	13.1	11.1	31.4	32.5	30.6	5.6	–4.7	1.6	–0.1	–3.2	0.7	2.9	–0.4
14	6.4	67.5	11.9	85.8	9.1	3.6	1.5	8.1	55.5	13.1	76.7	16.5	4.1	2.7	–1.7	12.0	–1.2	9.1	–7.4	–0.5	–1.3
15	3.4	4.9	68.9	77.3	4.9	13.8	4.1	0.0	4.4	77.3	81.7	4.2	10.8	3.2	3.4	0.5	–8.4	–4.5	0.7	3.0	0.9
16	9.0	3.3	11.1	23.4	64.1	5.6	6.9	7.6	3.7	7.3	18.6	65.7	7.4	8.2	1.4	–0.4	3.8	4.8	–1.6	–1.8	–1.3
17	2.6	20.5	5.5	28.6	7.6	63.9	0.0	0.0	18.4	10.6	29.0	10.8	60.3	0.0	2.6	2.1	–5.1	–0.4	–3.2	3.6	0.0

Note: Calculated values are averages based on analyses of three replicates per mineral mixture, using average peak areas from X-ray diffraction and normalization factors determined with matrix singular value decomposition (SVD).

Table T3. Linear regression equations and correlation coefficients for X-ray diffraction peak area vs. measured weight percent in standard mineral mixtures.

Mineral	Regression equation	Correlation coefficient
Smectite	$y = -0.55074 + 0.002472x$	r = 0.90365
Illite	$y = 1.843 + 0.0063395x$	r = 0.99359
Chlorite + kaolinite	$y = 5.3392 + 0.00074085x$	r = 0.92298
Quartz	$y = 1.0578 + 0.00081873x$	r = 0.95129
Plagioclase	$y = 1.3637 + 0.00092465x$	r = 0.97934
Calcite	$y = -2.3974 + 0.0017734x$	r = 0.98936

Note: y = peak area; x = weight percent.

Table T4. Calcareous nannofossil datums used, Leg 190.

Datum events	Species	Age (Ma)
FAD	*Emiliania huxleyi* acme	0.085
	Helicosphaera inversa	0.14
FAD	*Emiliania huxleyi*	0.26
LAD	*Pseudoemiliania lacunosa*	0.46
LAD	*Reticulofenestra asanoi*	0.88
FAD	*Reticulofenestra asanoi*	1.06
LAD	*Helicosphaera sellii*	1.46
LAD	*Calcidiscus macintyrei*	1.67
FAD	*Gephyrocapsa oceanica*	1.77
LAD	*Discoaster brouweri*	1.95
LAD	*Discoaster pentaradiatus*	2.52
LAD	*Discoaster surculus*	2.55
LAD	*Reticulofenestra pseudoumbilicus* (>7 µm)	3.8
LAD	*Amaurolithus* spp.	4.00
FCO	*Discoaster asymmetricus*	4.13
FAD	*Ceratolithus cristatus*	5.05
LAD	*Discoaster quinqueramus*	5.54
FAD	*Amaurolithus primus*	7.4
FAD	*Discoaster quinqueramus*	8.60
LAD	*Reticulofenestra pseudoumbilicus* (>7 µm)	9.0
LAD	*Discoaster hamatus*	9.63
FAD	*Discoaster hamatus*	10.7
FAD	*Catinaster coalitus*	10.9
LAD	*Discoaster kugleri*	11.5
FAD	*Discoaster kugleri*	11.8
LAD	*Orthorhabdus serratus*	12.3
LAD	*Sphenolithus heteromorphus*	13.6
LAD	*Helicosphaera ampliaperta*	15.6
LAD	*Sphenolithus belemnos*	19.2
FAD	*Sphenolithus belemnos*	19.2
FAD	*Discoaster druggii*	23.2

Note: FAD = first appearance datum; FCAD = first common appearance datum; LAD = last appearance datum.

Table T5. Wireline tool strings used and properties measured, Leg 190.

Tool string*	Typical logging speed (m/hr)	Tool*	Properties measured	Sample interval (cm)	Approximate vertical resolution (cm)	Approximate depth of investigation (cm)
Triple combination (total length = ~32 m)	250-275	HNGS	Natural gamma ray	15	45	Variable
		APS	Porosity	5 and 15	30	15
		HLDS	Bulk density, PEF	15	38	15
		DIT-SFL	Resistivity	15	150/90/60	150/76/38
		TAP	Temperature	1 per s	NA	NA
			Tool acceleration	4 per s		
			Pressure	1 per s		
FMS-sonic (total length = ~30 m)	25-275	NGS	Natural gamma ray	15	45	45
		GPIT	Tool orientation	1 or 15	NA	NA
		DSI	Sonic velocity	15	110	15–30
		FMS	Resistivity image	0.25	0.5	15

Notes: * = see Table T6, p. 51, for explanations of acronyms used to describe tool strings and individual tool names. PEF = photoelectric factor.

Table T6. Logging tool and measurement acronyms and units of measurement.

Tool	Output	Explanation	Units
HNGS		Hostile environment natural gamma-ray sonde	
	HSGR	Standard (total) gamma ray	API
	HCGR	Computed gamma ray (HSGR – uranium contribution)	API
	HFK	Formation potassium	Fractional %
	HTHO	Thorium	ppm
	HURA	Uranium	ppm
NGS		Natural gamma-ray sonde	
	SGR	Standard total gamma ray	API
	CGR	Computed gamma ray (SGR – uranium contribution)	API
	POTA	Potassium	%
	THOR	Thorium	ppm
	URAN	Uranium	ppm
APS		Accelerator porosity sonde	
	APLC	Near-array porosity (limestone corrected)	Fraction
	FPLC	Far-array porosity (limestone corrected)	Fraction
	SIGF	Neutron capture cross section of the formation (Sf)	cu
	STOF	Tool standoff (computed distance from borehole wall)	in
HLDS		High-temperature lithodensity sonde	
	RHOM	Bulk-density (corrected)	g/cm^3
	PEFL	Photoelectric effect	$barn/e^-$
	LCAL	Caliper: measure of borehole diameter	in
	DRH	Bulk-density correction	g/cm^3
DIT		Dual induction tool	
SFR		Spherically focused resistivity	
	IDPH	Deep induction phasor-processed resistivity	Ωm
	IMPH	Medium induction phasor-processed resistivity	Ωm
	SFLU	Shallow spherically focused resistivity	Ωm
GHMT		Geologic magnetic tool	
	MAGS	Magnetic susceptibility (limited range)	ppm
	RMGS	Low resistivity magnetic susceptibility (wider range)	ppm
	MAGC	Earth conductivity	ppm
	MAGB	Earth total magnetic field	nT
DSI		Dipole shear sonic imager	
	DTCO	Compressional wave transit time	µs/ft
	DTSM	Shear wave transit time	µs/ft
	DTST	Stoneley wave transit time	µs/ft
TAP		High-resolution temperature acceleration pressure tool	°C, mm/s^2, psi
GPIT		General purpose inclinometer cartridge	
	Fx, Fy, Fz	Magnetic field (three orthogonal directions)	nT
	Ax, Ay, Az	Acceleration (three orthogonal directions)	m/s^2